Title

Ethylene-regulated asymmetric growth of the petal base promotes flower opening in rose (Rosa hybrida)

Journal

The Plant Cell, 33(4)

ISSN

1040-4651

Authors

Cheng, Chenxia

Yu, Qin

Wang, Yaru

et al.

Publication Date

2021-05-31

DOI

10.1093/plcell/koab031

Peer reviewed

doi:10.1093/plcell/koab031

THE PLANT CELL

THE PLANT CELL 2021: 0: 1–23

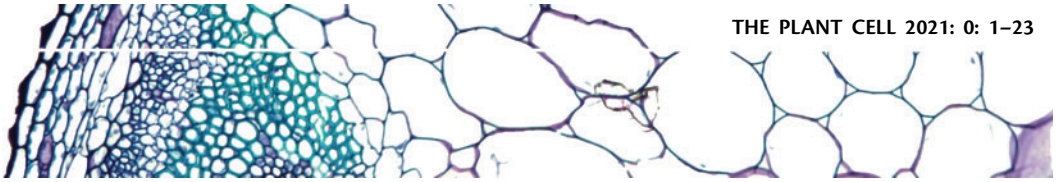

Research Article

Ethylene-regulated asymmetric growth of the petal base promotes flower opening in rose (*Rosa hybrida*)

Chenxia Cheng ,[1,†] Qin Yu ,[1] Yaru Wang ,[1] Hong Wang ,[1] Yuhan Dong ,[1] Yuqi Ji ,[1] Xiaofeng Zhou ,[1] Yonghong Li ,[2] Cai-Zhong Jiang ,[3,4] Su-Sheng Gan ,[5] Liangjun Zhao ,[1] Zhangjun Fei ,[6,7] Junping Gao [1] and Nan Ma [1,*,‡]

1 Department of Ornamental Horticulture, State Key Laboratory of Agrobiotechnology, Beijing Key Laboratory of Development and Quality Control of Ornamental Crops, China Agricultural University, Beijing 100193, China
2 School of Applied Chemistry and Biotechnology, Shenzhen Polytechnic, Shenzhen 518055, China
3 United States Department of Agriculture, Crop Pathology and Genetic Research Unit, Agricultural Research Service, Davis, California 95616
4 Department of Plant Sciences, University of California Davis, Davis, California 95616
5 Plant Biology Section, School of Integrative Plant Science, College of Agriculture and Life Sciences, Cornell University, Ithaca, New York 14853
6 Boyce Thompson Institute for Plant Research, Cornell University, Ithaca, New York 14853
7 USDA Robert W Holley Center for Agriculture and Health, Ithaca, New York 14853

*Author for communication: ma_nan@cau.edu.cn
†Present address: College of Horticulture, Qingdao Agricultural University, 700 Changcheng Road, Chengyang, Qingdao, Shandong, China
‡Senior author.
The author responsible for distribution of materials integral to the findings presented in this article in accordance with the policy described in the Instructions for Authors (www.plantcell.org) is: Nan Ma (ma_nan@cau.edu.cn).
C.C., Q.Y., Y.W., H.W., Y.D., and Y.J. performed the experiments. N.M. and J.G. designed the research. X.Z., Y.L., C.J., S.G., L.Z., Z.F., and N.M. provided the technical support, conceptual advice, and data analysis. C.C., J.G., and N.M. wrote the article.

Abstract

Flowers are the core reproductive structures and key distinguishing features of angiosperms. Flower opening to expose stamens and gynoecia is important in cases where pollinators much be attracted to promote cross-pollination, which can enhance reproductive success and species preservation. The floral opening process is accompanied by the coordinated movement of various floral organs, particularly petals. However, the mechanisms underlying petal movement and flower opening are not well understood. Here, we integrated anatomical, physiological, and molecular approaches to determine the petal movement regulatory network using rose (*Rosa hybrida*) as a model. We found that *PETAL MOVEMENT-RELATED PROTEIN1* (*RhPMP1*), a homeodomain transcription factor (TF) gene, is a direct target of ETHYLENE INSENSITIVE3, a TF that functions downstream of ethylene signaling. Rh*PMP1* expression was upregulated by ethylene and specifically activated endoreduplication of parenchyma cells on the adaxial side of the petal (ADSP) base by inducing the expression of Rh*APC3b*, a gene encoding the core subunit of the Anaphase-Promoting Complex. Cell expansion of the parenchyma on the ADSP base was subsequently enhanced, thus resulting in asymmetric growth of the petal base, leading to the typical epinastic movement of petals and flower opening. These findings provide insights into the pathway regulating petal movement and associated flower-opening mechanisms.

Received October 28, 2020. Accepted January 26, 2021. Advance access publication February 2, 2021

IN A NUTSHELL

Background: Flowers are unique structures in angiosperms that are used for reproduction. Proper flower opening is crucial for attracting pollinators and is pivotal for successful pollination. In general, flower opening is driven by the coordinated development and movements of floral organs, particularly petals. Time-lapse photography has shown that the movement of rose petals follows a smooth and continuous path, with outward movements at the petal base and a curvature towards the petal tops during opening. Many studies have shown that the gaseous phytohormone ethylene accelerates petal movement and flower opening in roses (*Rosa hybrida*).

Question: How does ethylene trigger the directional movement of petals?

Findings: Unexpectedly, we found that cell expansion-dependent growth of the adaxial side of the petal base, rather than expansion of the petal lamina, drives petal movement in rose. Ethylene accelerates petal movement by enhancing this asymmetric growth of the adaxial side of the petal base. PETAL MOVEMENT-RELATED PROTEIN1 (RhPMP1), a homeodomain transcription factor, is responsible for the asymmetric growth of the petal base during flower opening. RhPMP1 directly binds to the promoter of *ANAPHASE-PROMOTING COMPLEX 3b* (Rh*APC3b*), encoding a central player in cell endoreduplication. Both Rh*PMP1* and Rh*APC3b* are specifically induced by ethylene in the adaxial side of the petal base. Knockdown of either Rh*PMP1* or Rh*APC3b* impaired the ethylene-induced asymmetric growth of the petal base and petal movement.

Next steps: This work supports the notion that ethylene specifically activates a certain regulatory cascade (Rh*PMP1*-Rh*APC3b*) in the adaxial (but not abaxial) side of the petal bases of rose flowers. Considering the gaseous nature of ethylene, an interesting question is whether, and how, cell identity determines this unique response in the petal base.

Introduction

Flowers are unique structures in angiosperms that facilitate reproduction by providing a mechanism for the union of sperm cells with eggs. The time of flower opening, when anthers and pistils are visible, marks the onset of the period for attracting pollinators and consequent pollination. Many reports describe the mechanisms of flower initiation and organ differentiation, but much less is known about flower opening.

Flower opening which promotes pollination, is driven by the coordinated development and movements of floral organs, particularly petals (Reid and Evans, 1986; van Doorn and van Meeteren, 2003; Liang and Mahadevan, 2011; Srikanth and Schmid, 2011). This process can involve substantial growth and development. For example, from an unopened bud (Stage 1) to a fully opened flower (Stage 5), the fresh weight of rose (*Rosa hybrida*) petals increases approximately four-fold, and the petal area increases approximately six-fold (Ma et al., 2008; Yamada et al., 2009). Time-lapse photography has shown that the movement of rose petals follows a smooth and continuous path, with lateral (outward) movements at the petal base and a curvature toward the petal tops during opening.

Despite their sessile nature, plants are capable of moving to achieve specific developmental purposes and/or in response to environmental stimuli. More than a century ago, Darwin noted that the stems of all seedlings examined showed continuous circumnutation (Darwin and Darwin, 1880). He also described several typical movements in detail, including the sleep movement of leaves in legumes and phototropism and gravitropism of seedlings (Darwin and Darwin, 1880). Due to the lack of muscle cells, plant movement is usually driven by irreversible differential growth or by reversible changes in turgor pressure on different sides of organs (Chen et al., 2012; Forterre, 2013; Harmer and Brooks, 2018). Tropic movements, such as phototropism and gravitropism, are achieved through irreversible differential growth, which reorients organs to directional stimuli, such as light or gravity (Kiss, 2000; Liscum et al., 2014; Su et al., 2017). By contrast, plant movements that are induced by non-directional factors, such as temperature, humidity, or touch, are called nastic responses and are achieved through turgor-driven reversible movements. The phenomenon of "sleep movement of leaves" in legumes involves unfolding leaves or leaflets in the daytime and folding them at night: this typical nastic response is called nyctinasty (Chen et al., 2012).

Plant movement is controlled by multiple internal and external factors. One example is shoot phototropism, where the unequal redistribution of auxin across organs drives the movement (Liscum et al., 2014). In legumes, the nyctinastic movement of leaves or leaflets relies on a specialized structure: the so-called motor organ, or pulvinus, located at the base of the petiole of a single leaf, or the petiolules of leaflets in a compound leaf. The formation of the pulvinus is controlled by *ELONGATED PETIOLUTE1* (*ELP1*), a *LATERAL ORGAN BOUNDARIES* (*LBD*) transcription factor (TF) gene (Chen et al., 2012).

However, compared to shoot tropism and leaf nastic movement, the mechanism of petal movement and flower opening is not well understood, although the flower opening process has been extensively described for various species. In *Ipomoea*, daily movement of the corolla occurs due to movements of the midrib, which are driven by differences in cell expansion on both sides (Kaihara and Takimoto, 1981). In tulip (*Tulipa gesneriana*) and crocus (*Crocus sativus*), the opening and closure of tepals is sensitive to the ambient

temperature. Giving that water uptake-driven growth is faster on the inner vs. outer surfaces, an increase in temperature results in the outward movement of tepals and flower opening (Wood, 1953; Azad et al., 2004). In contrast to these reversible movements, flower opening in *Lilium* and rose (*R. hybrida*) is irreversible. In *Lilium*, flower opening is achieved through differences in growth between the petal margins and the midrib (Liang and Mahadevan, 2011).

To date, the regulatory mechanism of flower opening has not been well characterized. In this study, we chose rose (*R. hybrida*) as a model to investigate the regulatory network of flower opening and petal movement. Unexpectedly, we found that asymmetric growth of the petal base, rather than expansion of the petal lamina, drives petal movement. We show that the phytohormone ethylene accelerates petal movement by enhancing asymmetric growth of the petal base. The HD-Zip I subfamily TF, gene *PETAL MOVEMENT-RELATED PROTEIN1* (Rh*PMP1*) acts as a direct target of ETHYLENE INSENSITIVE3 (EIN3), the primary TF involved in ethylene signaling (Chao et al., 1997; Merchante et al., 2013). RhPMP1 induces the expression of *ANAPHASE-PROMOTING COMPLEX 3b* (Rh*APC3b*), thereby increasing the endoreduplication level of parenchyma cells on the adaxial side of the petal (ADSP) base, resulting in asymmetric growth of the petal base. Therefore, petal movement in rose is driven by the asymmetric growth of the petal base and is controlled by an Rh*PMP1*-Rh*APC3b* module in an ethylene-dependent manner, shedding light on the underlying regulatory mechanism of flower opening.

Results

Asymmetric growth of the petal base drives petal movement during flower opening in rose

Flower opening involves developmental changes in tissues adjacent to the flower and the coordinated movement of floral organs, especially petals (van Doorn and van Meeteren, 2003). A previous study suggested that rose flower opening depends on coordinated petal growth and movement (Reid and Evans, 1986). We observed the increases in size and outward movement of petals in different rose cultivars (Figure 1, A). In *Lilium*, petal unfolding is driven by the differential growth of the margins of petals and the midrib (Liang and Mahadevan, 2011). To determine whether differential growth of rose petals drives petal unfolding, we cut the top one-quarter, half, or three-quarters of the petals and monitored the flower opening process. Petal movement was not impaired in any of the cut flowers (Figure 1, B), and this outward petal movement was not disturbed when the flowers were cut vertically (Supplemental Movie S1). These results indicate that petal movement is independent of petal growth and may be controlled by the bottom part of the petals.

In legumes, the pulvinus structure in the petiole base controls leaf or leaflet movement by regulating the swelling and shrinking of cells on opposite sides (extensor and flexor) of the pulvinus (Chen et al., 2012; Cortizo and Laufs, 2012; Song et al., 2014). We monitored the development of rose petal bases using scanning electron microscopy and found that the petal base exhibited asymmetric growth during flower opening (Supplemental Figure S1). Next, we observed the growth of petal bases in longitudinal sections (Figure 2, A and B). The thickness of the petal base increased during flower opening (from Stages 1–5), especially in approximately the first 0.05–0.40 mm from the petal–receptacle junction (Figure 2, A–C). Based on these anatomical observations, we defined the upper part, namely the parenchyma tissue between the adaxial epidermis and the vascular bundles, as the ADSP, while the bottom part, namely the parenchyma tissue between the abaxial epidermis and the vascular bundles, as the abaxial side of the petals (ABSPs) (Figure 2, B, top).

In unopened floral buds (Stage 1), the thickness of the ADSP was similar to that of the ABSP (Figure 2, B, top panel; D and E). When the flowers started to open (Stage 3, partially opened flowers), the ADSP in the petal base exhibited a slight bump with larger cells (Figure 2, B, middle panel; D and E). Once the full opening was achieved (Stage 5), the ADSP formed an obvious bulge (Figure 2, B, bottom panel; D and E). To determine if the increase in thickness could be attributed to cell division or expansion, we measured the cell size and counted the cell numbers in petal bases. The cell size in the ADSP was significantly larger than in the ABSP in approximately the first 0.05–0.40 mm from the petal–receptacle junction at Stage 5 (Figure 2, F). The cell number of ADSP only slightly increased from Stages 1–3, which was limited to a narrow region closest to the petal–receptacle junction (Figure 2, G). Similar results were obtained when in vitro cultured plants were used (Supplemental Figure S2). These results suggest that petal movement in rose flowers is driven by the asymmetric growth of the petal base, primarily due to an increase in parenchyma cell size in the ADSP.

Ethylene accelerates flower opening by stimulating asymmetric growth of the petal base

Next, we investigated how the asymmetric growth of the petal base is regulated. Ethylene accelerates flower opening in roses (Reid et al., 1989; Ma et al., 2006; Ma et al., 2008; Xue et al., 2008), and ethylene production increases during flower opening and peaks at the fully opened stage (Ma et al., 2005; Pei et al., 2013). To determine whether the ethylene-induced flower opening is also driven by asymmetric growth of the petal base, we monitored the effects of ethylene and 1-MCP, an inhibitor of ethylene perception, on phenotypic and anatomical changes in petals. Consistent with previous reports, ethylene promoted flower opening, whereas 1-MCP did not cause obvious changes within 24 h of treatment (Supplemental Movie S2 and Figure 3, A). Analysis of cross-sections showed that ethylene significantly increased the thickness of the ADSP in the petal base, whereas 1-MCP slightly decreased it (Supplemental Figure S3). However, 1-MCP significantly

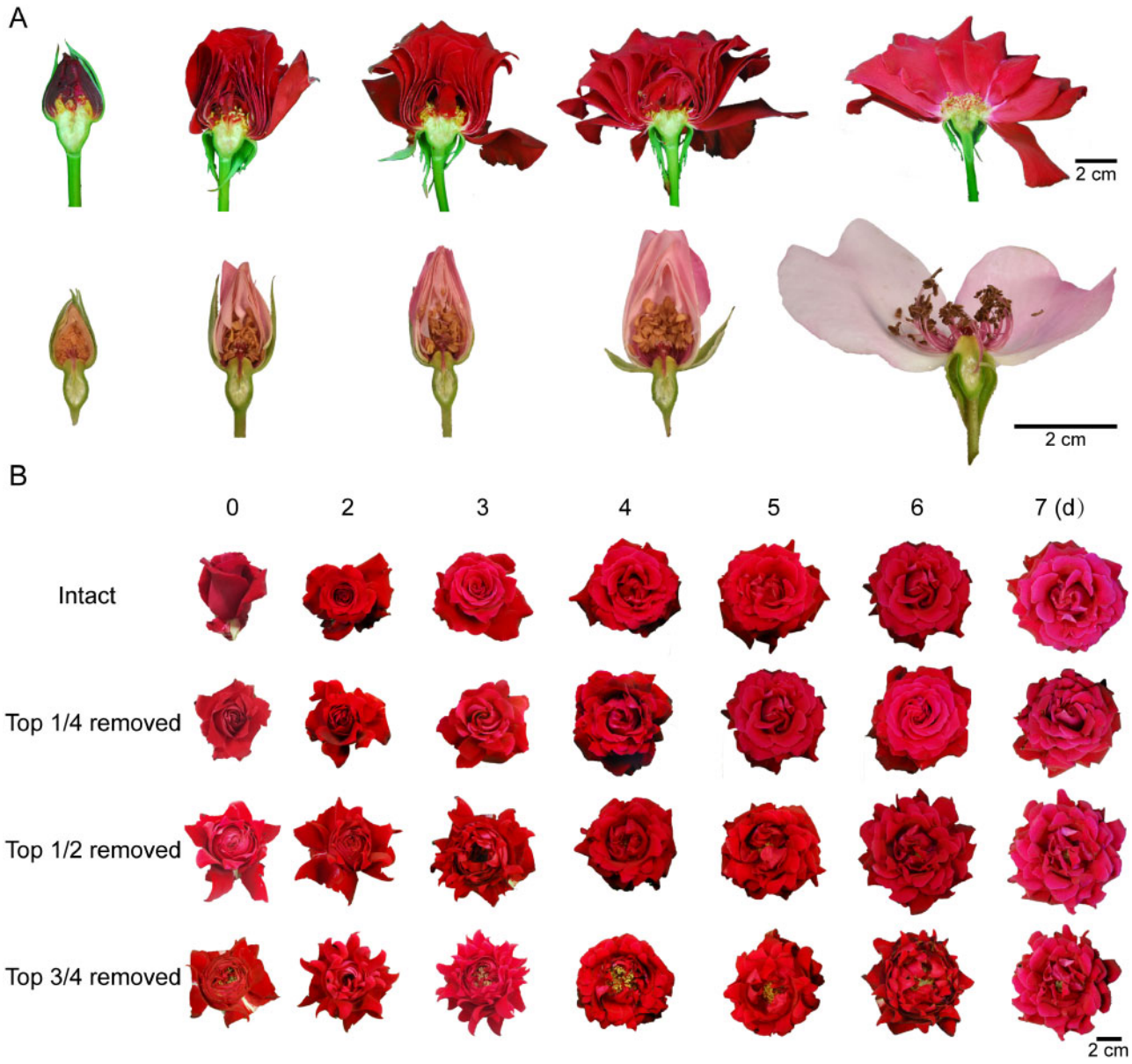

Figure 1 Growth of the petal lamina is not required for rose flower opening. A, Flower opening of rose double flowers (top, *R. hybrida* cv. Samantha) and single rose flowers (bottom, *R. hybrida* cv. Dainty Bess). The flowers were cut vertically during different stages of opening. B, Effects of the loss of the lamina on flower opening in *R. hybrid* cv. Samantha. Flowers were cut horizontally at the opened bud stage. one-quarter, half, or three-quarters represent the amount of the lamina that was removed from the top. Ten flowers were used for each treatment, and representative results are shown. Images of flowers were photographed separately at the scale indicated. Scale bar, 2 cm.

prolonged flower opening and weakened the outward movement of petals compared with untreated mock-control flowers (Supplemental Figure S4 and Supplemental Movie S3).

Interestingly, ethylene triggered the outward movement of the petals even when most of the petal lamina was cut off, supporting the idea that ethylene-induced petal movement is independent of petal lamina growth (Supplemental Figure S5). In longitudinal sections after 24 h of ethylene treatment, a bulge in the ADSP appeared at the petal base, phenocopying fully opened flowers (Figure 3, B). Ethylene specifically increased the thickness of the ADSP and the size of ADSP cells (Figure 3, C–E). There were fewer cells in the ADSP of ethylene-treated petals than the controls (Figure 3, F). Therefore, we propose that cell expansion is the major reason for ethylene-induced asymmetric growth of the petal base.

Silencing of Rh*PMP1* delays flower opening by impairing the asymmetric growth of the petal base

To identify putative regulators of asymmetric petal base growth, we performed RNA-seq analysis of ethylene-treated and control rose petal bases to identify differentially expressed genes (DEGs) in response to ethylene. A total of

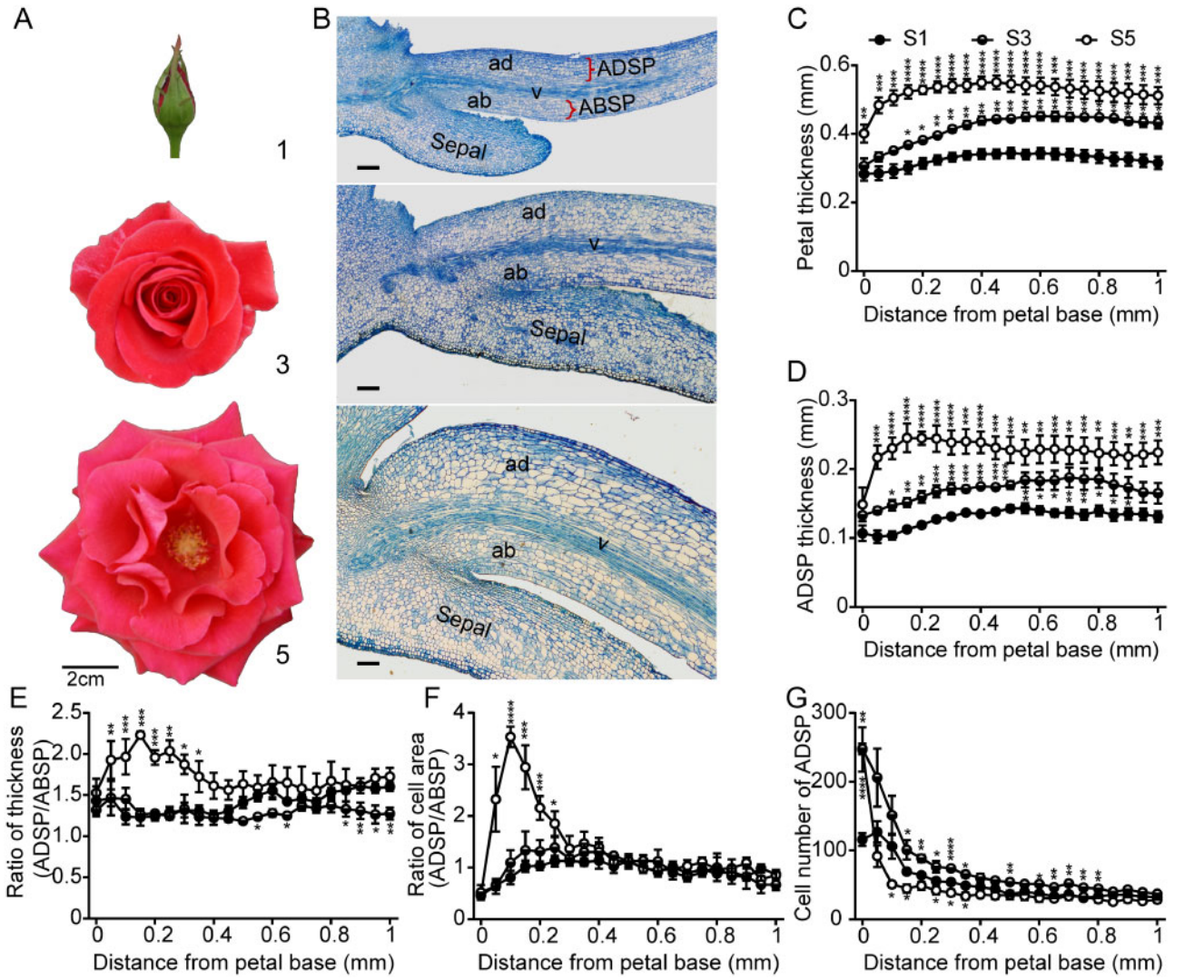

Figure 2 Flower opening is associated with asymmetric growth of the petal base. A and B, Flower phenotypes at different stages of opening (A) and longitudinal sections of petal bases (B) of flowers at the corresponding stages. 1, 3, and 5 indicate unopened buds, partially opened flowers, and fully opened flowers, respectively. Images of flowers were photographed separately at the scale indicated. Samples for anatomic analysis were harvested from the outermost petals. ab, abaxial side; ad, adaxial side; v, vascular bundle. Scale bar, 2 cm (A) and 100 μm (B). C and D, Thickness of petal bases (C) and ADSP (D) at Stages 1, 3, and 5. E and F, Ratio of thickness (ADSP/ABSP) (E) and cell size (ADSP/ABSP) (F) at Stages 1, 3, and 5. G, Cell numbers of ADSP at Stages 1, 3, and 5. The data were measured at the indicated distances from the petal-receptacle joint (0). S1, Stage 1; S3, Stage 3; S5, Stage 5. Closed symbols represent Stage 1, half-closed symbols represent Stage 3, and open symbols represent Stage 5. Values are mean ± SEM from at least three flowers. Asterisks indicate statistically significant differences compared to Stage 1. Student's *t* test, $^{*}P < 0.05$; $^{**}P < 0.01$; $^{***}P < 0.001$; $^{****}P < 0.0001$.

877 (P value $\leqslant 0.05$) TF genes were found to be differentially expressed (Figure 4, A and Supplemental Data Set S1). We chose 13 highly ethylene-responsive TF genes for further analysis. Quantitative reverse transcription polymerase chain reaction (qRT-PCR) analysis confirmed that expression of five genes (*RhWRKY20*, *RhSBP6*, *RhHD-ZIP*, *RhMYB41*, and *RhZIP41*) was highly induced by ethylene and correlated with the growth of the petal base during flower opening (Figure 4, B and C).

Using virus-induced gene silencing (VIGS), we individually silenced these five genes in rose plants and found that silencing of Rh*HD-ZIP* had a major effect on petal movement: thus, we renamed this gene Rh*PMP1* (Supplemental Figure S6, A and B). Silencing of Rh*PMP1* impaired ethylene-promoted flower opening and significantly weakened ethylene-induced cell expansion of ADSP in petal bases (Supplemental Figure S6, C–G). Rh*PMP1* is predicted to encode a 216 amino acid protein that contains a homeobox domain (HD) and a homeobox associated leucine zipper (HALZ) motif in its N-terminus (Supplemental Figure S7, A). Phylogenetic analysis indicated that Rh*PMP1* belongs to the HD-ZIP I subfamily and shares high sequence similarity with AT*HB7* and AT*HB12* from *Arabidopsis thaliana* (Figure 4, D). We expressed Rh*PMP1* fused to green fluorescence protein in *Nicotiana benthamiana* leaves and observed that the RhPMP1-GFP fusion protein localized to the nucleus

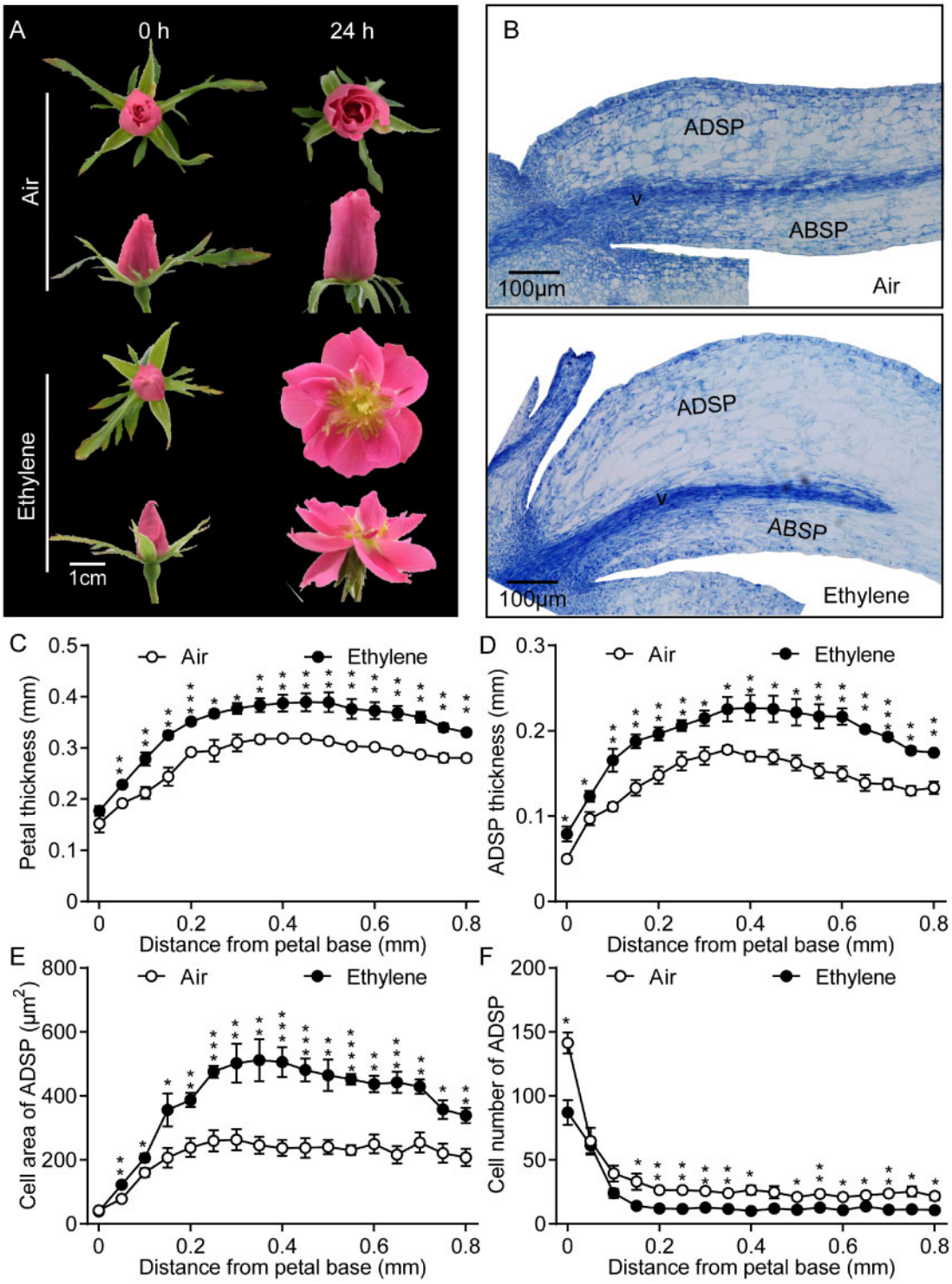

Figure 3 Ethylene accelerates flower opening by stimulating asymmetric growth of the petal base. A, Ethylene promotes flower opening. The opening phenotypes of rose flowers exposed to air or 10 μL L^{-1} ethylene for 24 h. Top (top) and side (bottom) views of flowers after air and ethylene treatments are shown. Images of flowers were photographed separately at the scale indicated. Scale bar, 1 cm. B, Longitudinal sections of petal bases of flowers after air (top) or 10 μL L^{-1} ethylene (bottom) treatment for 24 h. Scale bar, 100 μm. C–F, thickness of flower petal bases (C), thickness of ADSP (D), cell area (E), and cell number of ADSP (F). The data were measured at the indicated distances from the petal-receptacle joint (0). Values are mean ± SEM ($n \geqslant 3$). Student's *t* test, $^{*}P < 0.05$, $^{**}P < 0.01$, $^{***}P < 0.001$. v, vascular bundle.

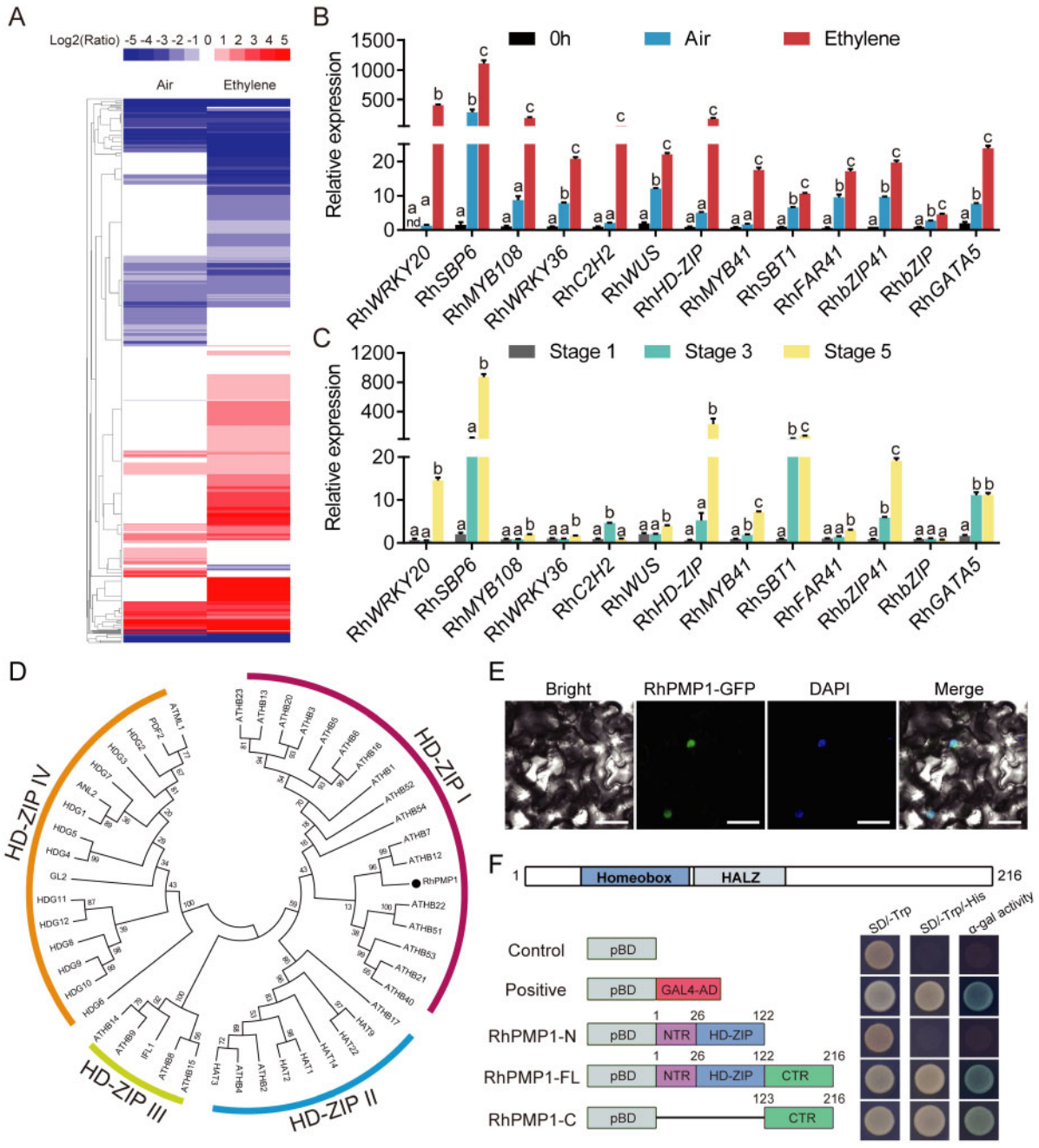

Figure 4 RhPMP1 is a transcription activator of HD-ZIP I subfamily. A, Ethylene-response profiles of 877 genes encoding transcriptional regulators in the petal base. Different shades of red and blue indicate the extent of the change according to the color bar provided (log2 ratio of 0 h). B, Validation of the highly ethylene-regulated genes by qRT-PCR. Rh*UBI2* (JK618216) was used as an internal control. The mean values ± SEM for four biological replicates are shown. Petal bases of the outmost layer petals of three flowers were pooled together as one biological replicate. Different letters above the bars indicate significant differences according to Duncan's multiple range test ($P < 0.05$). C, Expression patterns of selected genes expressed in petal bases as flowers open. Samples were harvested from the outermost petals at Stages 1, 3, and 5. Rh*UBI2* was used as an internal control. The mean values ± SEM are shown for four biological replicates. Petal bases of the outmost layer petals of three flowers were pooled together as one biological replicate. Different letters above the bars indicate significant differences according to Duncan's multiple range test ($P < 0.05$). D, A phylogenetic tree of RhPMP1 from rose and *A. thaliana* generated using MEGA version 6.0. Bootstrap values indicate the confidence of each branch. E, Subcellular localization of heterologously expressed RhPMP1-GFP in *N. benthamiana* leaves. DAPI staining was used to indicate the nuclei. Scale bar, 50 μm. The experiments were repeated twice, and representative results are shown. F, RhPMP1 transactivation assay. Top, schematic representation of RhPMP1. An HD and a HALZ motif were predicted by Conserved Domains Search (CD-Search, https://www.ncbi.nlm.nih.gov/Structure/cdd/wrpsb.cgi). Bottom, transactivation assay of RhPMP1 and its truncated versions in yeast. A series of RhPMP1 truncation fragments were fused to the GAL4-BD in pBD-GAL4 cam vector, as shown in the schematic representation. NTR, N-terminal residues, amino acids 1–26; HD-ZIP, amino acids 26 to 122; CTR, C-terminal residues, amino acids 122–216. The transactivation activity was verified by the growth of yeast AH109 harboring full-length and truncated fragments of RhPMP1 on SD/-Trp and SD/-Trp-His plates and was confirmed by a X-α-Gal staining assay.

(Figure 4, E). A transactivation assay indicated that the C-terminus of RhPMP1 has transcriptional activation activity in yeast (Figure 4, F), suggesting that it functions as a transcriptional activator.

To characterize the role of Rh*PMP1* in flower opening, we generated RNA interference lines of Rh*PMP1* (Rh*PMP1*-RNAi) in rose by *Agrobacterium*-mediated transformation (Supplemental Figure S8). We tested the effects of ethylene on flower opening in Rh*PMP1*-RNAi lines #4 and #2. In untreated plants, neither the flowers of wild-type (WT) nor Rh*PMP1*-RNAi plants opened. Treatment with ethylene for 24 h accelerated flower opening in WT plants, but did not lead to full flower opening in Rh*PMP1*-RNAi plants (Figure 5, A and B and Supplemental Movie S4). Analysis of both transverse (Figure 5, C) and longitudinal (Figure 5, F) sections showed that knockdown of Rh*PMP1* impaired the ethylene-promoted growth of ADSP in petal bases. In accordance with this phenotype, measurement of the thickness and cell size of petal bases supported the notion that ethylene-induced asymmetric growth was impaired in Rh*PMP1*-RNAi flowers (Figure 5, D, E, and G).

In situ hybridization demonstrated that Rh*PMP1* transcripts accumulated to a higher level in ADSP than in ABSP (Figure 6, A and B), further supporting the role of Rh*PMP1* in ethylene-induced asymmetric growth of petal bases. We also monitored the natural opening process of WT and Rh*PMP1*-RNAi flowers. Interestingly, knockdown of Rh*PMP1* significantly prolonged flower the opening process, just like the effects of 1-MCP treatment on flower opening (Supplemental Figures S4, S9). These findings suggest that Rh*PMP1* at least partially mediates the effects of ethylene on asymmetric petal base growth and participates in the control of flower opening.

Rh*PMP1* acts directly downstream from RhEIN3

Given that Rh*PMP1* expression is highly induced by ethylene, we searched the promoter of Rh*PMP1* for possible ethylene-responsive cis-elements using the PlantCare (https://sogo.dna.affrc.go.jp) and PlantPAN version 2.0 (http://plantpan2.itps.ncku.edu.tw/) databases. We found two putative EIN3 binding sites (EBS), "GCATGCAT" and "ACATGTAT," located at −489 bp to −497 bp and −1,383 bp to −1,391 bp, respectively, upstream from the start codon (ATG) (Supplemental Figure S7, B). Since EIN3 is a TF that acts as the primary and master regulator of the ethylene-signaling pathway (Chao et al., 1997; Merchante et al., 2013), we isolated the homolog of *EIN3* from rose (Rh*EIN3*). Sequence alignment showed that the putative amino acid sequence of RhEIN3 shares high similarity with known EIN3 proteins (Supplemental Figure S10, A); Knockdown of Rh*EIN3* in rose callus impaired ethylene-induced expression of Rh*ERF003* and Rh*PR10*, which are typical ethylene-responsive genes (Supplemental Figure S10, B), indicating that Rh*EIN3* plays an important role in mediating ethylene signaling in rose.

To test whether RhEIN3 directly binds to the promoter of Rh*PMP1*, we performed a yeast one-hybrid (Y1H) assay, confirming the binding of RhEIN3 to the distal EBS cis-element (Figure 7, A). An electrophoretic mobility shift assay (EMSA) further confirmed the specific binding of RhEIN3 to this EBS motif in vitro (Figure 7, B). To confirm the binding of RhEIN3 to the Rh*PMP1* promoter in planta, we conducted a chromatin immunoprecipitation (ChIP)-PCR assay by transiently expressing pSuper:Rh*EIN3-FLAG* in leaf mesophyll protoplasts isolated from transgenic *A. thaliana* leaves harboring ProRh*PMP1*:GUS. The results revealed a specific enrichment of RhEIN3 to the P5 region, which contained the distal EBS cis-element, in the Rh*PMP1* promoter (Figure 7, C).

We then tested the transactivation of the Rh*PMP1* promoter by RhEIN3 using the dual-LUC (firefly luciferase) reporter system. Co-transformation of *N. benthamiana* leaves with the 35S:Rh*EIN3* effector and the ProRh*PMP1*:*LUC* reporter led to significantly increased luciferase activity compared to the control (empty SK effector + ProRh*PMP1*:*LUC* reporter) (Figure 7, D). Live imaging revealed a strong luminescence signal in the region of *N. benthamiana* leaves that was co-transformed with the 35S:Rh*EIN3* and ProRh*PMP1*:*LUC* constructs (Figure 7, E). In addition, in situ hybridization showed that Rh*EIN3* was preferentially expressed in the ADSP of petal bases, similar to the expression pattern of Rh*PMP1* (Figure 6, C and D). These results indicate that RhEIN3 binds to and activates the Rh*PMP1* promoter.

The Rh*PMP1*-Rh*APC3b* module participates in petal movement by controlling cell endoreduplication

To understand how RhPMP1 regulates asymmetric petal base growth, we screened for possible target genes of RhPMP1 by conducting a comparative RNA-seq analysis of the petal bases from control and Rh*PMP1*-silenced plants. A total of 684 (P-value $\leqslant 0.05$ and fold-change $\geqslant 2$) genes were differentially expressed, including 201 upregulated and 483 downregulated genes (Supplemental Data Set S2). We measured the expression of the candidate genes in Rh*PMP1*-RNAi plants by qRT-PCR. Six cell expansion-related genes and one cell cycle-related gene were significantly downregulated in Rh*PMP1*-RNAi petal bases compared to the WT (Figure 8, A). We then tested for binding of RhPMP1 to the promoters of these seven genes using a Y1H assay. Unexpectedly, RhPMP1 directly bound to the promoter of the cell cycle-related gene Rh*APC3b*, but not to cell-expansion genes, such as *BETA-D-XYLOSIDASE* (Rh*BXL*), *PECTINESTERASE* (Rh*PE*), and *AQUAPORIN* (Rh*PIP2;1*) (Figure 8, B and Supplemental Figure S11, A). The open-reading frame (ORF) of Rh*APC3b* is 2,292-bp long and encodes a putative 763 amino acid residue protein. Phylogenetic analysis using the protein sequences of APC members from *A. thaliana* showed that RhAPC3b is most closely related to AtAPC3b (Supplemental Figure S11, B). Conserved domain analysis identified an ANAPHASE-PROMOTING COMPLEX, CYCLOSOME, SUBUNIT 3 domain, and eight tetratricopeptide repeat domains, which are consistent with the characteristics of APC proteins (Heyman and De Veylder, 2012; Eloy et al., 2015;

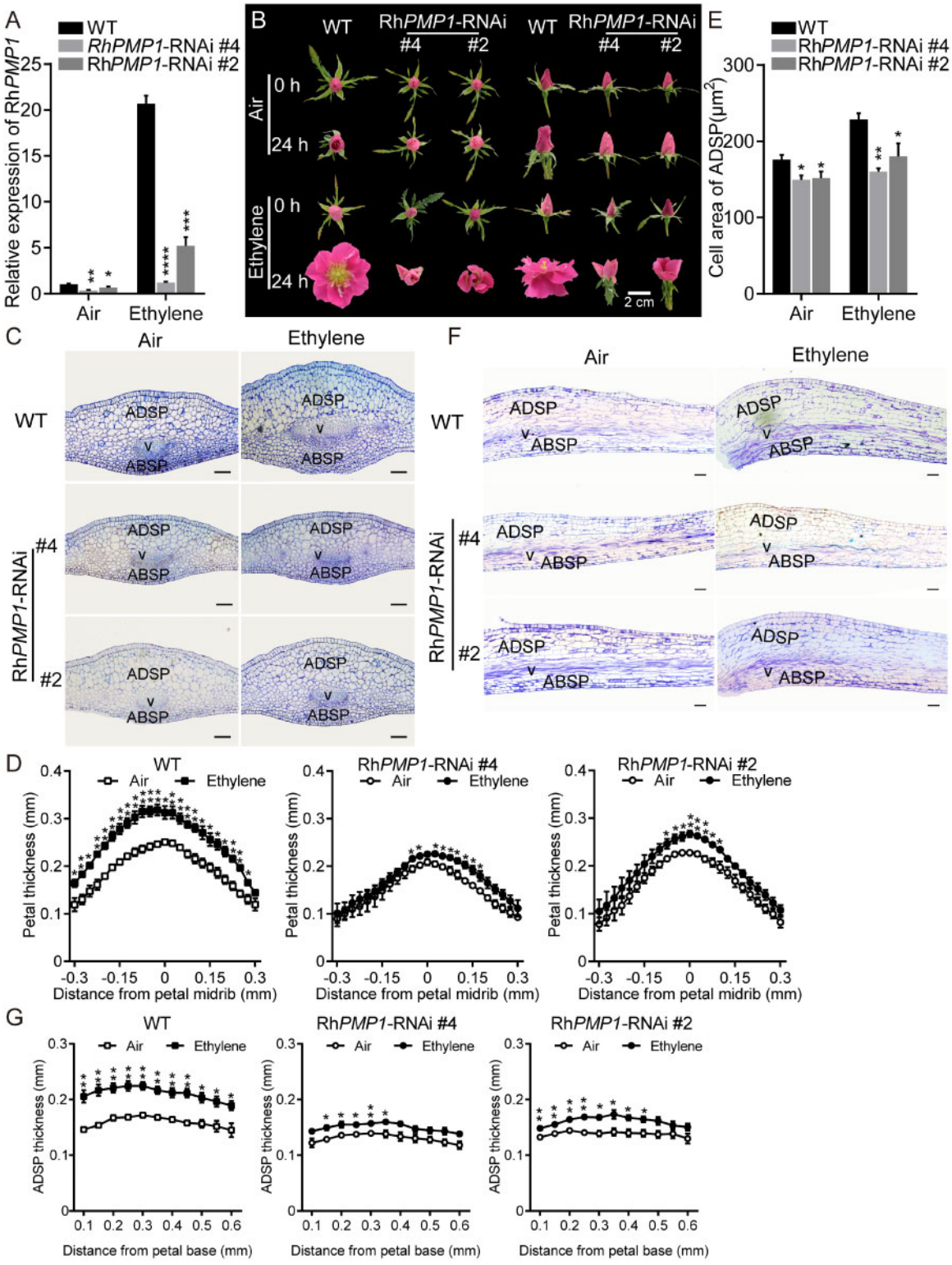

Figure 5 Knockdown of Rh*PMP1* by RNA interference impairs ethylene-promoted flower opening. A, qRT-PCR analysis of Rh*PMP1* expression in response to ethylene in petal bases of WT and Rh*PMP1*-RNAi lines. Flowers (opened buds) were exposed to air or 10 μL L^{-1} ethylene for 24 h. Rh*UBI2* was used as an internal control. The mean values ± SEM are shown for three biological replicates. Petal bases of at least six flowers (two petal of outmost layer were used for each flower) were pooled together as one biological replicate. Student's *t*-test, $^{*}P < 0.05$; $^{**}P < 0.01$; $^{****}P < 0.0001$. B, Knockdown of Rh*PMP1* inhibits the ethylene-induced full opening of flowers. Top (left) and side (right) view of flowers after air and ethylene treatments. Flowers (opened bud stage) were exposed to air or 10 μL L^{-1} ethylene for 24 h. Images of flowers were photographed separately at the scale indicated. Scale bar, 2 cm. The experiments were performed independently 3 times, and similar results were obtained. For each experiment, at least 10 WT plants and 10 Rh*PMP1*-RNAi plants were used ($n \geq 10$). The representative results from one experiment are shown for morphology (B) and anatomical structure (C, F). C–E, Transverse sections (C), thickness of petal bases (D), and cell area of ADSP (E) of

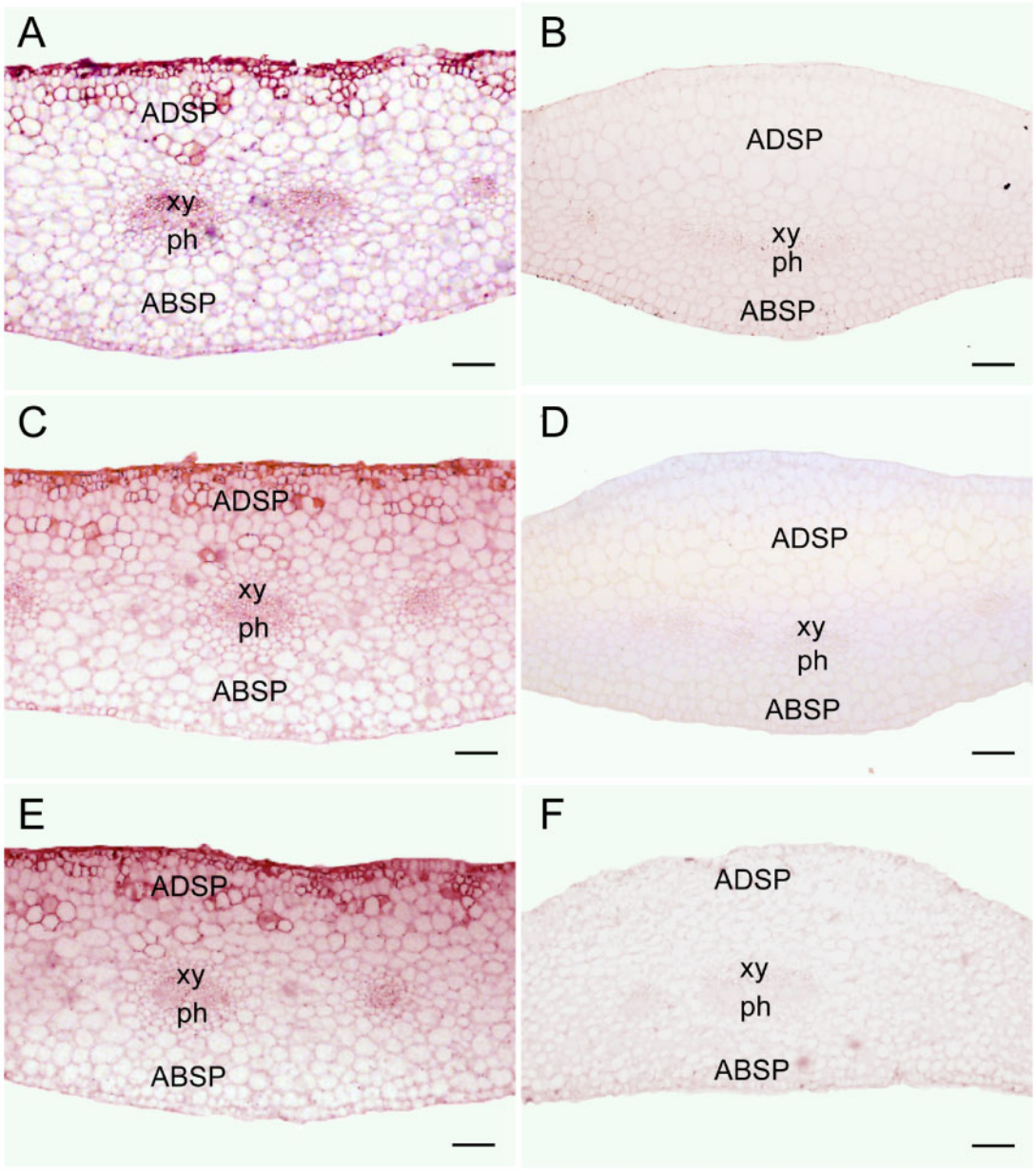

Figure 6 Expression patterns of RhEIN3, RhPMP1, and RhAPC3b in petal bases. In situ hybridization with an antisense probe of RhPMP1 (A), RhEIN3 (C), and RhAPC3b (E), as well as a sense probe of RhPMP1 (B), RhEIN3 (D), and RhAPC3b (E). Images show transverse sections of petal bases. Scale bar, 50 μm. xy, xylem; ph, phloem.

Supplemental Figure S11, C, top). Fluorescence localization demonstrated that RhAPC3b localizes to the nucleus (Supplemental Figure S11, C, bottom), which is consistent with the known role of APC proteins in regulating mitotic and endoreduplication cycles in eukaryotes (Reed, 2003).

Analysis of the Rh*APC3b* promoter identified two putative HD-ZIP I TF-binding sites, CAATCATTG (−281 to −290) and TAATAATTC (−350 to −359) (Palena et al., 2001; Ariel et al., 2007; Figure 8, B, top). An Y1H assay showed that RhPMP1 activates the promoter of Rh*APC3b* (Figure 8, B, bottom).

WT and Rh*PMP1*-RNAi plants. Scale bar, 50 μm. The thickness of petal bases was measured after air and ethylene treatments. Values are mean ± SEM (n = 3). Student's t test, $^{*}P < 0.05$; $^{**}P < 0.01$. F and G, Longitudinal sections (F) and thickness of ADSP in petal bases (G) of WT and Rh*PMP1*-RNAi lines. Scale bar, 50 μm. The thickness of ADSP in petal bases was measured after air and ethylene treatments. Values are mean ± SEM (n = 3). Student's t-test, $^{*}P < 0.05$; $^{**}P < 0.01$.

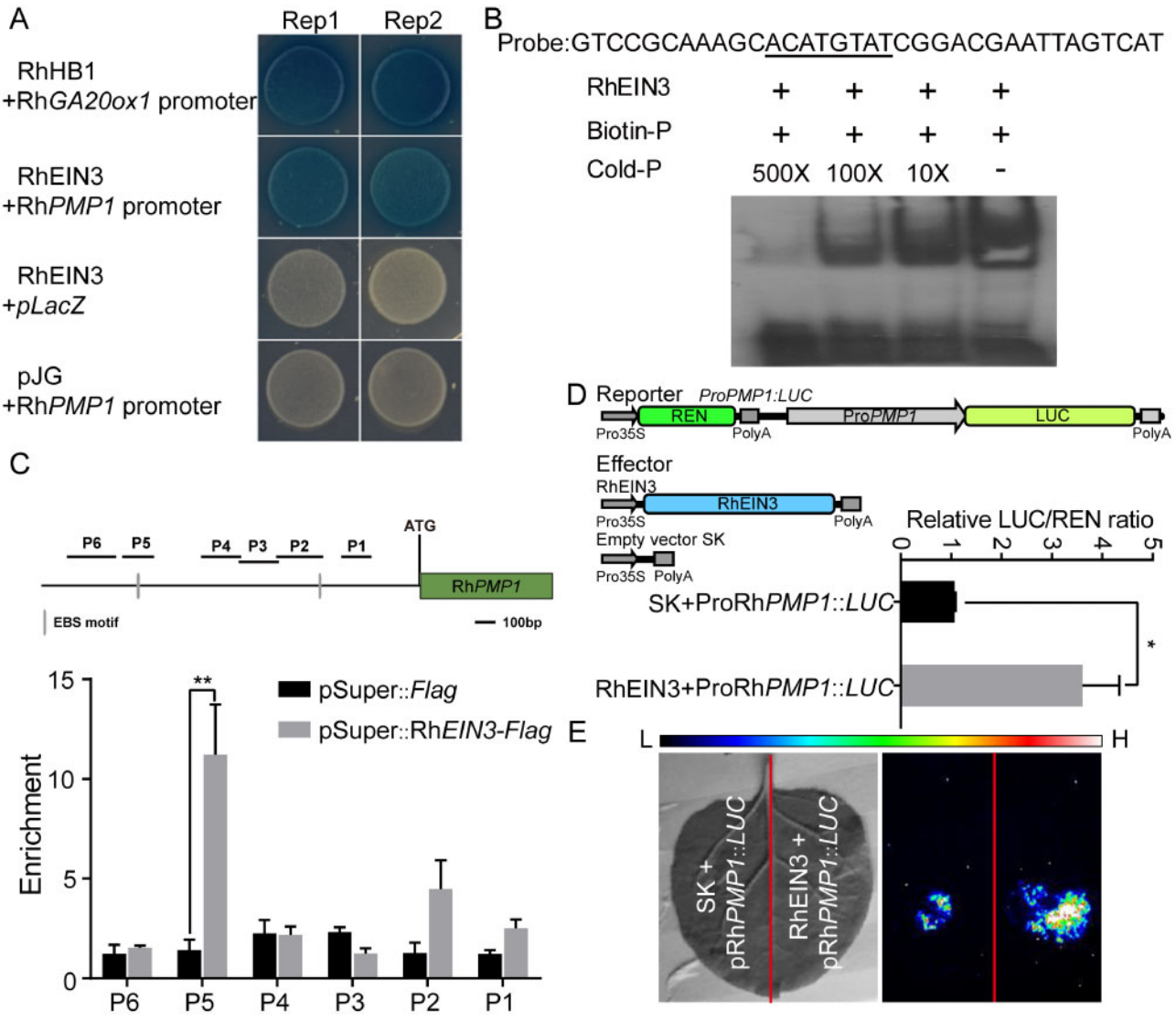

Figure 7 RhPMP1 acts directly downstream from RhEIN3. A, Y1H assay showing RhEIN3 binding to the Rh*PMP1* promoter. Both RhEIN3 + pLacZ and pJG + the Rh*PMP1* promoter were used as negative controls. RhHB1 + the Rh*GA20ox1* promoter was used as a positive control. Replicates 1 and 2, two technical replicates. B, EMSA of interactions between RhEIN3 and the Rh*PMP1* promoter. The probe was designed from a fragment of the Rh*PMP1* promoter containing the distal EBS motif (−1382 to −1392bp). Purified GST-tagged RhEIN3 protein (3 μg) was incubated with 20 nM of biotin-labeled probe. Non-labeled probe at 10-, 100-, and 500-fold was added for the competition test. C, ChIP-PCR assay showing RhEIN3 binding to the Rh*PMP1* promoter in planta. Top, schematic representation of the Rh*PMP1* promoter sequence. Green box, Rh*PMP1* ORF; Gray vertical lines, the putative EBS motifs; Lines above, the fragments amplified in the ChIP-PCR analysis. P1: −13 to −262 bp, P2: −471 to −715 bp, P4: −692 to −897 bp, P4: −875 to −1,082 bp, P5: −1304 to −1,471 bp, P6: −1,439 to −1,738 bp, relative to the Rh*PMP1* translation initiation codon (ATG). Bottom, ChIP-enrichment of the indicated Rh*PMP1* promoter fragments (P1–P6). Three-week-old transgenic *A. thaliana* plants harboring ProRh*PMP1*:*GUS* were used for isolation of leaf mesophyll protoplasts. The pSuper:Rh*EIN3-FLAG* and pSuper:*FLAG* (negative control) plasmids were separately transfected into the protoplasts. The experiment was performed independently 3 times, and representative results are shown. The mean values ± SEM are shown from four biological replicates. Each infected tube of protoplasts was considered to be one biological replicate. Student's *t* test, $^{**}P < 0.01$. D, Dual-luciferase activity assay showing transactivation of the Rh*PMP1* promoter by RhEIN3. Top, schematic representation of the effector and reporter constructs. Bottom, the dual-luciferase activity assay. A 1,740 bp Rh*PMP1* promoter region (0 to −1,740) was used in this assay. 35S:Rh*EIN3* and ProRh*PMP1*:*LUC* were co-infiltrated into *N. benthamiana* leaves. Three independent transfection experiments were performed, and representative results are shown. Values are mean ± SEM. Student's *t*-test, $^{*}P < 0.05$. E, Live imaging of *N. benthamiana* leaves expressing Rh*EIN3* and ProRh*PMP1*:*LUC*. Leaves harboring the empty vector (SK) and the Rh*PMP1* promoter were used as a negative control. The color scale represents the signal density. H, high; L, low. The experiment was performed independently 3 times, and representative results are shown.

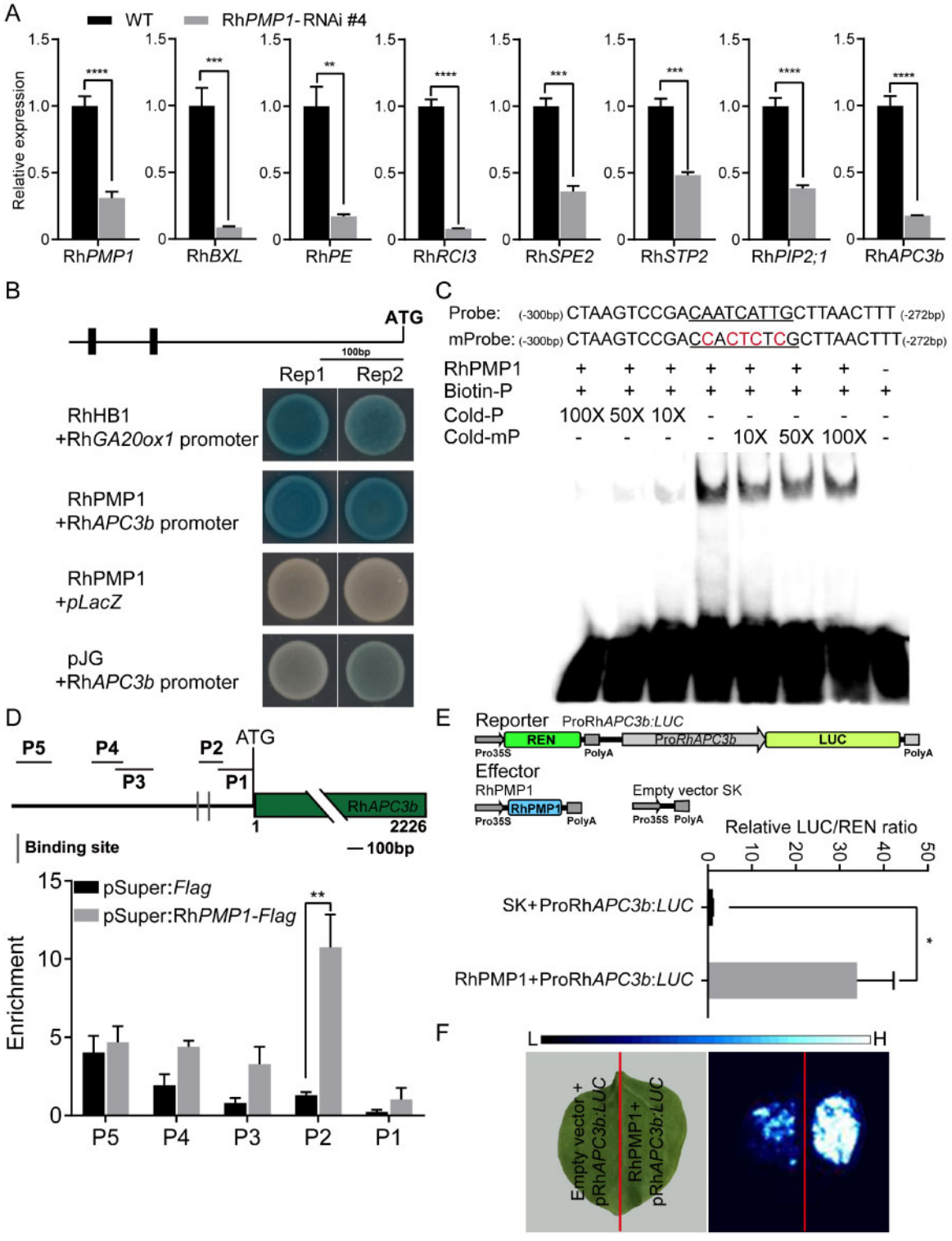

Figure 8 RhPMP1 directly regulates Rh*APC3b* expression. A, qRT-PCR of putative Rh*PMP1* downstream genes in petal bases of WT and Rh*PMP1*-RNAi plants. The expression of Rh*BXL*, Rh*PE*, Rh*RCI3*, Rh*SPE2*, Rh*STP2*, and Rh*PIP2;1* (plasma membrane intrinsic protein 2;1), and Rh*APC3b* was tested. Rh*UBI2* was used as an internal control. The mean values ± SEM are shown from four biological replicates. Petal bases of the outmost layer petals of three flowers were pooled together as one biological replicate. Student's *t* test, $^{**}P < 0.01$; $^{***}P < 0.001$; $^{****}P < 0.0001$. B, Y1H assay showing RhPMP1 binding to the Rh*APC3b* promoter. Top, schematic representation of the Rh*APC3b* promoter sequence. Black vertical lines, the putative HD-ZIP I TF target motifs. Both RhPMP1 + pLacZ and pJG + the Rh*APC3b* promoter were used as negative controls. RhHB1 + the Rh*GA20ox1* promoter was used as a positive control. Replicates 1 and 2, two technical replicates. C, EMSA of interactions between RhPMP1 and the Rh*APC3b* promoter. The probe was designed from a fragment of the Rh*APC3b* promoter containing the RhPMP1 binding site (−272 to −300 bp). Purified GST-tagged RhPMP1 protein (3 μg) was incubated with 20 nM of biotin-labeled probe. Non-labeled probe (Cold-P) and Non-labeled mutated probe (Cold-mP) at 10-, 50-, and 100-fold were added for the competition test. The experiment was performed independently 3 times,

An EMSA demonstrated that mutation of the CAATCATTG *cis*-element abolished the specific binding of RhPMP1 to the Rh*APC3b* promoter (Figure 8, C). ChIP-PCR analysis revealed that RhPMP1 specifically bound to the P2 fragment of the Rh*APC3b* promoter in planta (Figure 8, D), which contains these two predicted cis-elements. A quantitative luciferase activity assay and live imaging of *N. benthamiana* leaves co-transformed with the 35S:Rh*PMP1* effector and the ProRh*APC3b*:*LUC* reporter confirmed the finding that RhPMP1 activates the expression of ProRh*APC3b*:*LUC* (Figure 8, E and F). These results indicate that RhPMP1 is a direct upstream transactivator of Rh*APC3b*. Interesingly, a Y1H and an EMSA showed that RhEIN3 could directly bind to the promoter of Rh*APC3b* and activate it as well (Supplemental Figure S12, A and B).

Knockdown of Rh*APC3b* delays ethylene-induced flower opening by affecting asymmetric petal base growth

qRT-PCR analysis indicated that the expression pattern of Rh*APC3b* is similar to that of Rh*PMP1*: Rh*APC3b* expression increased in the ADSP of the petal base as the flower opened and was highly induced in the ADSP by ethylene treatment (Supplemental Figure S12, C and D). In situ hybridization demonstrated that the region of Rh*APC3b* expression overlapped with that of Rh*PMP1* in the petal base (Figure 6, E and F), suggesting that Rh*APC3b* might function with Rh*PMP1*.

To elucidate the role of Rh*APC3b* in petal movement, we silenced Rh*APC3b* in rose using VIGS. Phenotypic and anatomical analysis showed that silencing of Rh*APC3b* impaired ethylene-promoted flower opening and asymmetric growth of the ADSP in petal bases (Supplemental Figure S13). We then created Rh*APC3b*-RNAi lines by *Agrobacterium*-mediated transformation (Supplemental Figure S14). We observed the effects of ethylene on petal movement and flower opening of *RhAPC3b*-RNAi line #6 and #5 plants. Ethylene treatment for 24 h accelerated flower opening in WT plants as before, but only slightly affected flower opening in Rh*APC3b*-RNAi plants (Figure 9, A and B and Supplemental Movie S5), an effect similar to that in Rh*PMP1*-RNAi plants (Figure 5, B). Analysis of both transverse (Figure 9, C) and longitudinal (Figure 9, F) sections showed that ethylene-enhanced asymmetric petal base growth was much weaker in Rh*APC3b*-RNAi plants than in the WT, with substantially reduced thickness and cell size in the ADSP of Rh*APC3b*-RNAi flowers (Figure 9, D, E, and G).

These findings suggest that the Rh*PMP1*-Rh*APC3b* regulatory module controls ethylene-induced flower opening by regulating asymmetric petal base growth. Interestingly, qRT-PCR showed that not all genes that were downregulated in Rh*PMP1*-RNAi plants were downregulated in Rh*APC3b*-silenced plants (Supplemental Figure S12, D), indicating that Rh*APC3b* might simply function in one branch of the RhPMP1-regulated gene network. Similar to the Rh*PMP1*-RNAi lines, the Rh*APC3b*-RNAi lines also showed a delayed natural flower opening process (Supplemental Figure S15).

In *A. thaliana*, the *APC3b* mutant *hobbit* (*hbt*) exhibits decreased cell division and cell size and a reduced number of cells with high ploidy levels due to a defect in endoreduplication (Blilou et al., 2002; Serralbo et al., 2006). This raised the question of whether the Rh*PMP1*-Rh*APC3b* module also controls cell size and asymmetric growth of the petal base by regulating cell endoreduplication in petal bases. To address this question, we first generated Rh*PMP1*-overexpressing (ox) and Rh*APC3b*-ox *A. thaliana* lines. Both Rh*PMP1*-ox and Rh*APC3b*-ox lines exhibited larger leaves than WT Columbia-0 (Col-0) plants (Supplemental Figures S16, A, 17, A). We then measured nuclear DNA content in the leaves of 10-day-old transgenic *A. thaliana* plants harboring Rh*PMP1* or Rh*APC3b* by flow cytometry and observed a reduction in the proportion of 2C cells but increases in 8C, 16C, and 32C cells in both Rh*PMP1*-ox and Rh*APC3b*-ox lines (Supplemental Figures S16, B, S17, B). These results indicate that the Rh*PMP1*-Rh*APC3b* module acts as a positive regulator of ploidy levels in the transgenic *A. thaliana*. Flow cytometry analysis further showed that the proportion of 4C cells increased in the petal base as the flower opened and reached the maximum level at the fully opened stage (Figure 10, A). In addition, ethylene treatment significantly increased the proportion of 4C cells in the petal base (Figure 10, B).

Taken together, our results reveal that ethylene induces the expression of the Rh*PMP1*-Rh*APC3b* module, thus promoting the asymmetric growth of petal bases by

and representative results are shown. D, ChIP-PCR assay of the binding of RhPMP1 to the Rh*APC3b* promoter in planta. Top, schematic representation of the Rh*APC3b* promoter sequence. Green box, Rh*APC3b* ORF; Gray vertical lines, the putative HD-ZIP I TF target motifs; Lines above, the fragments amplified in the ChIP-PCR analysis. P1: −1 to −226 bp, P2: −127 to −345 bp, P3: −623 to −836 bp, P4: −815 to −1,007 bp, P5: −1,259 to −1,475 bp, relative to ATG of *RhAPC3b*. Bottom, ChIP-enrichment of the indicated the *RhAPC3b* promoter fragments (P1–P5). Three-week-old transgenic *A. thaliana* plants harboring ProRh*APC3b*:*GUS* were used as a source of leaf mesophyll protoplasts. pSuper:Rh*PMP1-FLAG* and pSuper:*FLAG* (negative control) plasmids were separately transfected into the protoplasts. The experiment was performed 3 times, and representative results are shown. The mean values ± SEM from three biological replicates are shown. Each infected tube of protoplasts was considered to be one biological replicate. Student's *t* test, $^{**}P < 0.01$. E, Dual-luciferase activity assay of RhPMP1 transactivation of the Rh*APC3b* promoter. 35S:Rh*PMP1* and ProRh*APC3b*:*LUC* were co-infiltrated into *N. benthamiana* leaves. Top, schematic representation of the effector and reporter constructs. Bottom, the dual-luciferase activity assay. Three independent transfection experiments were performed. Values are mean ± SEM. Student's *t* test, $^{*}P < 0.05$. F, Live imaging of *N. benthamiana* leaves expressing Rh*PMP1* and ProRh*APC3b*:*LUC*. The 1,744 bp Rh*APC3b* promoter (0 to −1,744) was used. Leaves harboring the empty vector (SK) and the Rh*APC3b* promoter were used as a negative control. The color scale represents the signal density. The experiment was performed independently 3 times, and representative results are shown.

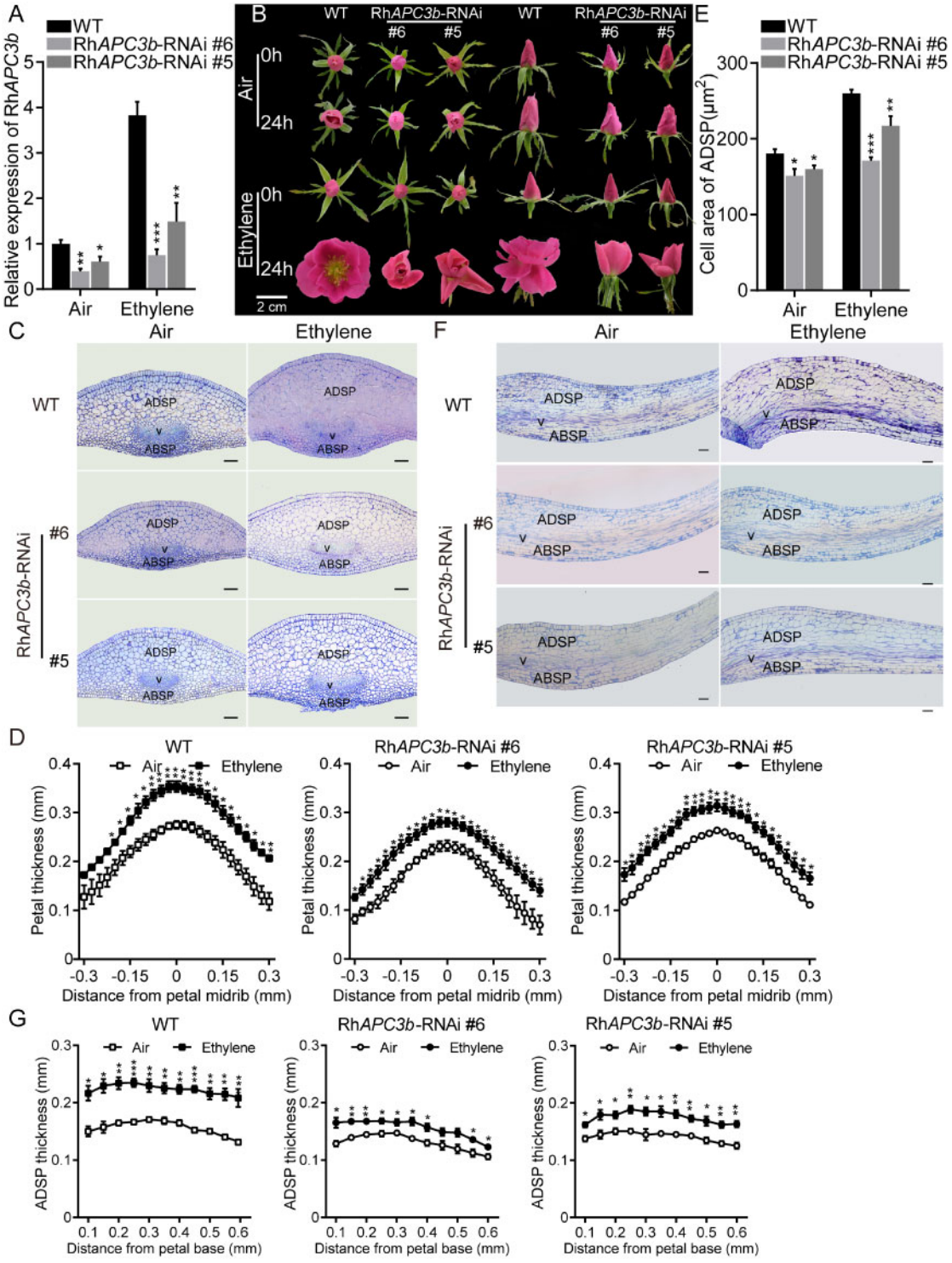

Figure 9 Knockdown of Rh*APC3b* by RNA interference impairs ethylene-promoted flower opening and asymmetric growth of petal base. A, qRT-PCR analysis of Rh*APC3b* in response to ethylene in petal bases of WT and Rh*APC3b*-RNAi lines. Flowers (opened buds) were exposed to air or 10 μL L^{-1} ethylene for 24 h. Rh*UBI2* was used as an internal control. The mean values ± SEM from three biological replicates are shown. Petal bases of at least six flowers (two petal of outmost layer were used for each flower) were pooled together as one biological replicate. Student's *t*-test, $^{*}P < 0.05$; $^{**}P < 0.01$; $^{***}P < 0.001$. B, Knockdown of Rh*APC3b* inhibits ethylene-induced full flower opening. Top (left) and side (right) view of flowers after air and ethylene treatments. Images of flowers were photographed separately at the scale indicated. Scale bar, 2 cm. The experiments were performed independently 3 times, and similar results were obtained. For each experiment, at least 10 WT plants and 10 Rh*APC3b*-RNAi plants were used ($n \geqslant 10$). The representative results from one experiment are shown for morphology (B) and anatomical structure (C, F). C–E, Transverse sections (C), thickness of petal bases (D), and cell size of ADSP (E) of WT and Rh*APC3b*-RNAi lines. Scale bar, 50 μm. The petal base thickness was measured after air and ethylene treatment. Values are mean ± SEM ($n = 3$). Student's *t* test, $^{*}P < 0.05$; $^{**}P < 0.01$; $^{***}P < 0.001$. F and G, Longitudinal sections (F) and thickness of ADSP in petal bases (G) of WT and Rh*APC3b*-RNAi lines. Scale bar, 50 μm. The thickness of ADSP at the petal base was measured after air and ethylene treatments. Values are mean ± SEM ($n = 3$). Student's *t* test, $^{*}P < 0.05$; $^{**}P < 0.01$; $^{***}P < 0.001$.

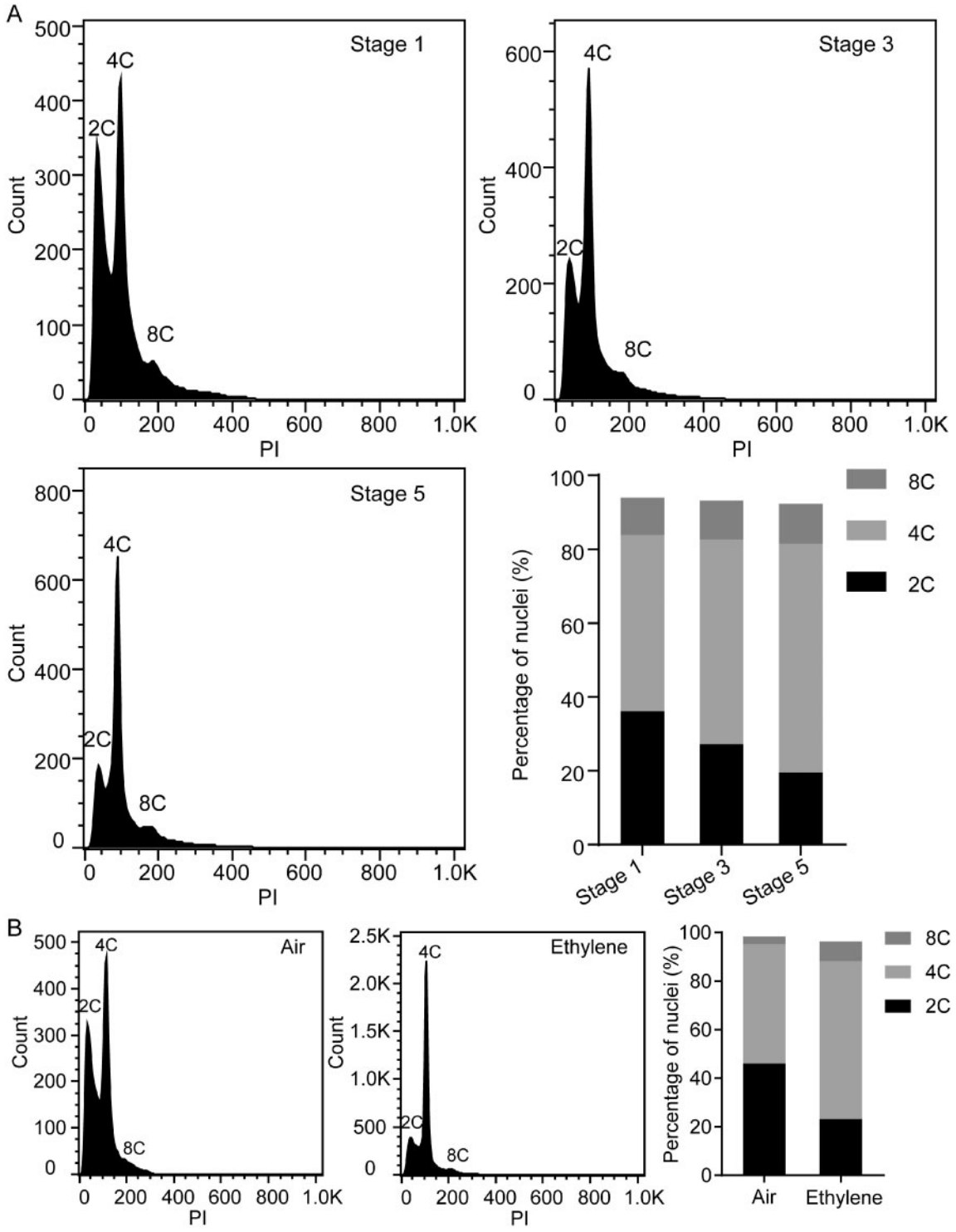

Figure 10 Ploidy levels of ADSP cells at the petal base during flower opening and in response to ethylene. A, Flow cytometry histograms of ADSP cells in the petal bases of flowers at Stages 1, 3, and 5. The relative ratio of cells at each ploidy level in the petal base ADSP at different stages of flower opening. B, Flow cytometry histograms of ADSP cells at the petal base in control (air) and ethylene-treated flowers (Ethylene). Flowers (opened buds) were exposed to air or 10 μL L^{-1} ethylene for 24 h. (PI was used to stain nuclei in chopped petal base tissues. The data are representative of three independent experiments.

enhancing the endoreduplication of ADSP cells, ultimately resulting in petal movement and flower opening (Supplemental Figure S18).

Discussion

Flowering can be divided into several major phases: the transition from the shoot apical meristem to the floral meristem;

the determination and formation of floral organs; and flower opening leading to pollination (Lang, 1952). The mechanisms of flower opening have not been determined, especially at the genetic and molecular levels, although it is known to be a complex process that is tightly regulated by various internal and external cues (Reid and Evans, 1986; van Doorn and van Meeteren, 2003; Liang and Mahadevan, 2011; Van Doorn and Kamdee, 2014).

In this current study, we identified a gene network that is responsible for ethylene-induced petal movement and flower opening using rose as a model. Ethylene triggers asymmetric petal base growth, which drives irreversible petal movement (Supplemental Figure S18). This ethylene-induced process is dependent on a unique structure resulting from the asymmetric growth of petal bases that could be considered an epinastic movement (Kang, 1979). This structure is, to some extent, similar to that of the motor organ/pulvinus, which is located at the bases of petioles or petiolules in legumes such as pea (*Pisum sativum*), barrel medic (*Medicago truncatula*), and *Lotus japonicas* (Darwin and Darwin, 1880; Chen et al., 2012). In the motor organ/pulvinus, changes in turgor pressure in cells at opposite sides (extensors and flexors) of the pulvinus mediate nyctinastic movement of leaves or leaflets (Cote, 1995; Moran et al., 1996; Moran, 2015). The LBD TF ELP1, which is conserved in legumes, regulates the development of the pulvinus. In WT *M. truncatula*, the pulvinus is a short cylindrical structure with radial symmetry consisting of isodiametric and identical cortical cells. In the loss-of-function mutant *elp1-1*, pulvinus development is defect and the pulvinus-specific cells are replaced by rachis- or petiole-like cells, resulting in the failure of leaflet folding in the dark (Chen et al., 2012). Unlike the pulvinus in legumes, the asymmetric structure located at the petal base of roses drives irreversible petal unfolding, and the formation of this structure is associated with petal movement.

The diffusion of ethylene is generally considered to be random due to its gaseous nature. The unequal distribution of ethylene has been reported only in some unique circumstances, such as in response to flooding. Under waterlogged conditions, ethylene diffusion from submerged tissues is substantially reduced due to the diffusion barrier resulting from the surrounding water. Consequently, the endogenous ethylene concentration significantly increases, which triggers both hyponasty and non-differential linear petiole or internode elongation in marsh dock (*Rumex palustris*) and *A. thaliana* (Jackson, 1985; van Zanten et al., 2010; Polko et al., 2011; Voesenek and Bailey-Serres, 2015). Ethylene is thought to cause rapid acidification of the apoplast and upregulation of genes encoding the cell wall loosening proteins expansins (Vriezen et al., 2000; Vreeburg et al., 2005), which are favorable for rapid cell expansion. In addition, in *A. thaliana*, ethylene accumulation stimulates the reorientation of cortical microtubules from longitudinal to transverse at the abaxial sides of petioles to direct longitudinal cell expansion, leading to leaf hyponasty (Polko et al., 2012). Ethylene can also control the amplitude of hyponasty by attenuating cell proliferation of the abaxial side of the petiole by downregulating *CYCA2;1*, an A2-type cyclin gene (Polko et al., 2015).

Notably, exogenous ethylene is sufficient to mimic the submerged-induced hyponasty response in *R. palustris* and *A. thaliana*, suggesting that unique ethylene distribution patterns are not required for this process (Millenaar et al., 2005; Pierik et al., 2006; Polko et al., 2012, 2015). This petiole hyponasty response is similar to our observations of rose flower petal movements, although the latter is an epinastic movement. Here, we provided evidence that ethylene influences the epinastic movement of petals by activating endoreduplication-induced cell expansion on the ADSP base by upregulating the Rh*EIN3*-Rh*PMP1*-Rh*APC3b* module. Rh*APC3b* is a rose homolog of *A. thaliana APC3b/HOBBIT*, which encodes an indispensable subunit of the Anaphase-Promoting Complex/Cyclosome (APC/C complex) and is expressed during the S/G2-M phases of the cell cycle. The APC/C complex consists of 17 subunits of three types: the core subunits; the catalytic subunits; and the activator subunits. APC3b/HOBBIT is a core subunit that physically interacts with most other subunits (Heyman and De Veylder, 2012; Eloy et al., 2015). The *APC3b/HOBBIT* loss-of-function mutant *hbt* exhibits reduced cell size and number and a defect in endoreduplication, with fewer cells with high ploidy levels (Serralbo et al., 2006; Pérez-Pérez et al., 2008).

In rose, Rh*APC3b* is upregulated by ethylene through the Rh*EIN3*-Rh*PMP1* module. Knockdown of Rh*APC3b* or Rh*PMP1* attenuated cell expansion on the ADSPs and weakened asymmetric petal base growth. Rh*PMP1*-RNAi and Rh*APC3b*-RNAi plants exhibited prolonged flower opening, which mimics the effects of 1-MCP on flower opening, suggesting that the Rh*PMP1*-Rh*APC3b* module plays a central role in ethylene-induced petal movement and flower opening. Interestingly, 1-MCP treatment or knockdown of Rh*PMP1*/Rh*APC3b* significantly prolonged the opening process but did not completely block flower opening, pointing to the existence of an alternative, perhaps secondary pathway that regulates flower opening.

Meanwhile, knockdown of Rh*PMP1* or Rh*APC3b* resulted in smaller flowers compared to WT plants. Conversely, overexpression of either Rh*APC3b* or Rh*PMP1* significantly increased the proportion of cells with high ploidy levels and leaf size in transgenic *A. thaliana*. Further analyses will be required to provide a more in depth understanding of the mechanism by which the Rh*PMP1*-Rh*APC3b* module regulates organ size.

In addition, the ploidy levels of cells in the petal base increased as the flowers opened and were elevated by ethylene treatment. Ethylene treatment stimulates cell endoreduplication in *A. thaliana* and cucumber (*Cucumis sativus*) hypocotyls (Gendreau et al., 1999; Dan et al., 2003). Here, we demonstrated that ethylene regulates cell endoreduplication and thus influences cell expansion in rose petal bases through a transcriptional cascade involving Rh*EIN3*-Rh*PMP1*-Rh*APC3b*. Intriguingly, we previously found that ethylene

treatment inhibited cell expansion in the petal lamina (Ma et al., 2005; Pei et al., 2013). Moreover, even in the petal base, ethylene dramatically induced cell expansion by enhancing endoreduplication in the adaxial side but not in the abaxial side. In situ hybridization also demonstrated that all three genes, Rh*EIN3*, Rh*PMP1*, and Rh*APC3b*, displayed a similar pattern of transcript distribution, namely, preferentially accumulating in the ADSP region. These findings suggest that ethylene specifically activates a certain regulatory cascade in the ADSP but not the ABSP. Considering the gaseous nature of ethylene, it would be interesting to explore whether, and how, cell identity determines this unique response.

Materials and methods

Plant materials and growth conditions

Cut rose (*R. hybrida* cv. Samantha) flowers were harvested from a local commercial greenhouse, immediately placed in tap water, and delivered to the laboratory within 1 h. The stems were re-cut under water to a length of 25 cm, and uniform flowers without any defects were selected and kept in deionized water until further processing. The stages of cut flower opening were defined as previously described (Ma et al., 2005). Floral organ samples were collected at different stages of opening, and petal samples were collected from the same middle whorl of flowers.

Arabidopsis thaliana ecotype Col-0 seeds were surface sterilized, sown on Murashige and Skoog (MS) medium, and stratified at 4°C for 3 days to promote germination. After vernalization, the seeds were transferred to a growth chamber for 7 days. Seven-day-old seedlings were transplanted into growth mixture (vermiculite/nutritive soil = 1:1) and grown under the following conditions: 22 ± 2°C, 50% relative humidity and 100–120 μmol m^{-2} s^{-1} illumination with fluorescent lamps (SINOL, SN-T5, 16 W) under a 16/8-h light/dark cycle.

For ethylene or 1-MCP treatment, rose flowers (opening Stage 2) were exposed to 10 μL L^{-1} ethylene or 2 μL L^{-1} 1-MCP in an airtight chamber for 24 h. For continuous treatment, the flowers (opening Stage 2) were exposed to air or 2 μL L^{-1} 1-MCP in an airtight chamber until the flowers opened. The air and 1-MCP in the chambers were refreshed every 24 h to avoid possible side effects. NaOH solution (1 M) was present in the chamber to prevent CO_2 accumulation (Ma et al., 2006).

Histological analysis

Paraffin sections of petal bases were prepared as previously described (Cheng et al., 2013), with some modifications. Petal bases containing part of the receptacle were collected, fixed in FAA solution (formaldehyde:70% ethanol:acetic acid, 5:90:5 [v/v/v]) overnight at room temperature, and stored at 4°C until further use. Semi-thin sections were prepared as previously described (Pinon et al., 2008), but with some modifications. Petal bases were fixed in 2.5% glutaraldehyde, dehydrated through an acetone series to 100% acetone, and embedded in Low Viscosity Embedding Kit (Spurr) resin (EMS, PA, USA). The embedded tissue was sectioned (3 μm sections) using a Leica RM2265 (Leica Microsystems, Wetzlar, Germany) rotary microtome, placed on microscopy slides, and stained with 0.02% Toluidine Blue in 100 mM Phosphate buffer (pH 7.2). The slides were observed under an optical microscope (OLYMPUS BH-2, Tokyo, Japan) and photographed with a digital camera (OLYMPUS DP72, Japan). Cell counts and cell sizes were determined using ImageJ and Photoshop software.

Rose transformation

For the Rh*PMP1* RNAi construct, two primer sets with different restriction enzyme sites were used to amplify a 351 bp fragment (483–834 bp). One set, with *Asc* I and *Swa* I sites, was digested and inserted in sense orientation into the pFGC1008 vector; the other, with *Pac* I and *Bam* HI sites, was digested and inserted in antisense orientation into the pFGC1008 vector. Similarly, a 284 bp fragment (793–1,077 bp) was used to generate the Rh*APC3b* RNAi construct.

Transgenic rose plants were generated as described previously with minor modifications (Liu et al., 2020). Briefly, unexpanded leaves with three leaflets were used to induce somatic embryogenesis in the dark in Somatic Embryo Induction Medium (SIM, MS + 3.0 mg L^{-1} 2.4 – D + 0.05 mg L^{-1} KT + 60 g L^{-1} glucose + 20 g L^{-1} mannitol + 2.5 g L^{-1} GEL). The RNAi construct was introduced into *Agrobacterium* strain EHA105 and grown overnight. The bacteria were collected by centrifugation and re-suspended in infiltration solution (MS + 45 g L^{-1} glucose + 100 μmol L^{-1} acetosyringone). The bacterial suspension was adjusted with infiltration solution to an OD_{600} = 0.5 and incubated for 2 h at 28°C with shaking (200 rpm). The somatic embryos were immersed in the bacterial suspension and incubated for 40 min at 28°C with shaking (180 rpm). The somatic embryos were briefly washed and dried on sterilized paper towels to remove excess bacterium solution. The somatic embryos were incubated on Co-cultivation Medium (CM, MS + 1.0 mg L^{-1} 2, 4-D + 0.05 mg L^{-1} 6-benzylaminopurine (6-BA) + 60 g L^{-1} glucose + 2.5 g L^{-1} GEL + 100 mg L^{-1} casein hydrolysate + 100 μmol L^{-1} acetosyringone) at 22 ± 1°C in the dark for 3 days without selection. The somatic embryos were selected on Selective Germination Medium (SGM, half MS + 1.0 mg L^{-1} 6-BA + 0.01 mg L^{-1} α-naphthalene acetic acid (NAA) + 0.5 mg L^{-1} gibberellic acid (GA_3) + 300 mg L^{-1} Cef + 30 mg L^{-1} Hygromycin B + 100 mg L^{-1} Casein hydrolysate + 30 g L^{-1} Glucose + 2.5 g L^{-1} GEL + 20 g L^{-1} Mannitol). The somatic embryos were repeatedly transferred to a fresh SGM every 2 weeks. When resistant shoots appeared, they were transferred to Selective Rooting Medium (SRM, half MS + 1.0 mg L^{-1} NAA + 30 mg L^{-1} Hygromycin B + 30 g L^{-1} Sucrose + 7.5 g L^{-1} GEL) to induce root formation. Each single shoot was considered to be an independent line. The rooted plants were transferred to pots containing a 1:1 volume of peat moss and vermiculite and grown at 22 ± 1°C with RH 60% and 100–120 μmol m^{-2} s^{-1} illumination with

fluorescent lamps (SINOL, SN-T5, 16 W) under a 16-h light/8-h dark photoperiod. Positive transformants were screened according to the presence of the selective gene (Hyg) and the T-DNA insert. qRT-PCR was carried out to assess the expression of Rh*PMP1* or Rh*APC3b* in the transgenic lines. Primer sequences are listed in Supplemental Data Set S3.

In situ hybridization

In situ hybridization was performed as described previously (Ma et al., 2008; Ma et al., 2015). The petal bases were fixed in freshly prepared, cold 4% (w/v) paraformaldehyde by vacuum infiltration for 25 min (repeated once) and incubated overnight at 4°C. The samples were dehydrated through a graded ethanol series (50%–100%) and embedded in Paraplast plus (Sigma, St. Louis, MO, USA). Antisense and sense probes of Rh*EIN3*, Rh*PMP1*, and Rh*APC3b* were amplified from gene-specific regions and labeled using a digoxigenin (DIG)-RNA labeling kit (Roche, Basel, Switzerland). Sections were processed and incubated with DIG-labeled RNA probe overnight at 50°C. Anti-DIG conjugated to alkaline phosphatase was used to detect DIG-labeled RNA. Images were photographed under an optical microscope (OLYMPUS BH-2, Japan). Primer sequences are listed in Supplemental Data Set S3.

Y1H assay

The Rh*EIN3* ORF was cloned into the *Eco*R I and *Sal* I sites of the pJG4-5 vector (Clontech Laboratories, Inc., Mountain View, CA, USA), resulting in the GAD-RhEIN3 construct. The Rh*PMP1* ORF was cloned into the *Eco*R I and *Xho* I sites of the pJG4-5 vector, resulting in the GAD- RhPMP1 construct. To generate a construct expressing the LacZ reporter gene driven by the Rh*PMP1* or Rh*APC3b* promoter, a 36-bp oligonucleotide (5′-AGATGTCCGCAAAGCACATGTATCGG ACGAATTAGT-3′) from the Rh*PMP1* promoter was synthesized and the Rh*APC3b* fragment (−389 to −1 bp from the Rh*APC3b* ATG start codon) was amplified from *R. hybrid* cv. Samantha genomic DNA before being cloned into the pLacZi2μ vector. The fragments of the other gene promoters Rh*BXL*/*RHL36571*, Rh*PE*/*RHL35830*, *PEROXIDASE 3* (Rh*RCI3*)/*RHL03332*, Rh*PIP2;1*/GenBank No. EU572717, *SUGAR PHOSPHATE EXCHANGER 2* (Rh*SPE2*)/*RHL36450*, and *SUGAR TRANSPORTER2* (Rh*STP2*)/*RHL26676*, were amplified from *R. hybrid* cv. Samantha genomic DNA and cloned into the pLacZi2μ vector.

Y1H assays were performed as previously described (Lin et al., 2007). Briefly, a plasmid expressing the GAD-RhPMP1 or GAD-EIN3 fusion was co-transformed with various *LacZ* reporter gene constructs into yeast strain EGY48 as described in the Yeast Protocols Handbook (Clontech Laboratories, Inc.). Transformants were grown on synthetic dextrose plates lacking uracil and tryptophan but containing X-Gal to observe color development. RhHB1 + the Rh*GA20ox1* promoter was used as a positive control (Lü et al., 2014). The primers used are listed in Supplemental Data Set S3.

EMSA

The EMSA was performed as described previously (Pei et al., 2013). For prokaryotic expression of RhEIN3, the ORF of Rh*EIN3* was inserted into the *Sma* I and *Sal* I sites of the pGEX-4T-2 vector to generate the pGEX-4T-Rh*EIN3* plasmid. For prokaryotic expression of RhPMP1, the ORF of Rh*PMP1* was inserted into the *Eco* RI and *Xho* I sites of the pGEX-4T-2 vector to generate the pGEX-4T-Rh*PMP1* plasmid. Recombinant GST-RhEIN3 and GST-RhPMP1 fusion proteins were produced in *Escherichia coli* strain BL21, and protein production was induced by adding isopropyl-β-D-thiogalactopyranoside and incubating at 28°C for 6 h. The *E. coli* cells were lysed by sonication. The GST-RhEIN3 and GST-RhPMP1 proteins were purified with Glutathione-Sepharose 4B beads (GE Healthcare, Chicago, IL, USA) according to the manufacturer's instructions. The ProRh*PMP1* probe 5′-GT CCGCAAAGCACATGTATCGGACGAATTAGTCAT-3′ and the ProRh*APC3b* probe 5′-CTAAGTCCGACAATCATTGC TTAACTTT-3′ were synthesized and labeled with biotin. Unlabeled DNA of the same sequence was used as a competitor. To prepare double-stranded DNA probes, the oligonucleotides were dissolved in TE buffer (10 mM Tris pH 8.0, 1 mM EDTA) at a concentration of 1–5 OD/100 μL mixed at the same molar ratio, incubated 94°C for 5 min, cooled at room temperature, and stored at −20°C. EMSA was performed using a Light Shift Chemiluminescent EMSA kit (Pierce, Rockford, IL, USA), according to the manufacturer's instructions. All primers used are listed in Supplemental Data Set S3.

ChIP-PCR assay

For ChIP-PCR analysis, the Rh*PMP1* ORF containing *Sal* I and *Spe* I restriction sites, and the Rh*EIN3* ORF containing *Sal* I and *Spe* I sites, were separately inserted into the pSuper:*FLAG* vector to generate pSuper:Rh*PMP1-FLAG* and pSuper:Rh*EIN3-FLAG*, respectively. ChIP assays were performed using *A. thaliana* (Col-0) protoplasts isolated from 3-week-old leaves and transformed with the Rh*PMP1* or Rh*APC3b* promoter as previously described (Pei et al., 2013). The pSuper:Rh*PMP1-FLAG* and pSuper:Rh*EIN3-FLAG* plasmids were transfected into protoplasts containing ProRh*APC3b*:*GUS* and ProRh*PMP1*:*GUS*, respectively. Following incubation at room temperature for 20 h, the protoplasts were fixed using 1% (v/v) formaldehyde. The chromatin complexes from the fixed protoplasts were fragmented by sonication and incubated with anti-FLAG® M2 Magnetic Beads (M8823; Sigma) for 6 h. After washing, the eluted samples were incubated at 65°C for 6 h to reverse the cross-linking. The co-precipitated DNA was purified and analyzed using qRT-PCR. Each ChIP assay was repeated three times. The primers used for vector construction and ChIP-qPCR are listed in Supplemental Data Set S3.

Flow cytometry

Flow cytometry was performed using a Moflo XDP analyzer for Arabidopsis seedlings (Beckman Coulter, Brea, CA, USA) or BD FACSCalibur (Becton Dickinson, USA) for rose petal

bases. *A. thaliana* seedlings or rose petal bases were chopped in 200 µL LB01 buffer (15 mM Tris, 2 mM Na_2EDTA, 0.5 mM spermine tetrahydrochloride, 80 mM KCl, 20 mM NaCl, 0.1% (v/v) Triton X-100, pH 7.5) with a single-sided razor blade in a Petri dish (Doležel et al., 2007). Filters were prepared using a 1 mL pipette tip and a 50 µm nylon mesh. Six-hundred microliter ice-cold LB01 buffer was added to the Petri dish containing the chopped tissue, and the liquid was transferred into a 5 mL polystyrene round-bottomed tube (Corning Science, Mexico S.A. de C.V.) through the filter. The nuclei were collected by centrifuging horizontally at 100 *g* for 5 min. The supernatant was carefully removed and 300 µL LB01 buffer containing 50 mg mL^{-1} propidium iodide (PI) and 50 mg mL^{-1} RNase A was added. After 30 min, the nuclei were analyzed. DNA histograms were drawn and the ploidy levels were calculated using FlowJo software.

RNA-seq

Strand-specific RNA-seq libraries were constructed as previously described (Zhong et al., 2011), and three biological replicates for each treatment were sequenced on an Illumina HiSeq 2000 system using the single-end mode. RNA-seq reads were first aligned to assembled rose transcripts using Bowtie (Zhong et al., 2011), allowing one mismatch. Following alignment, raw counts for each rose transcript in each sample were derived and normalized to reads per kilobase of exon model per million mapped reads. Genes that were differentially expressed (fold change $\geqslant 2.0$ and adjusted *P*-value < 0.05) between Rh*PMP1*-silenced and TRV control samples were identified using the DESeq package (Anders and Huber, 2010).

VIGS

For the VIGS assay, rose plants were propagated by in vitro culturing. Rose shoots of at least 2 cm, including one node, were cultured on propagation medium (MS medium containing 1.0 mg L^{-1} 6-BA, 0.05 mg L^{-1} NAA, and 1.0 mg L^{-1} GA_3 for 30 days and transferred to rooting medium (half-strength MS supplemented with 0.1 mg L^{-1} NAA) for 30 days. The flower opening stages of in vitro cultured rose plants were defined as previously described (Wu et al., 2017).

For Rh*PMP1* and Rh*APC3b* silencing, an Rh*PMP1*-specific (507 bp in length) and a Rh*APC3b*-specific (440 bp in length) fragment was PCR-amplified to generate the pTRV2-Rh*PMP1* and pTRV2-Rh*APC3b* construct, respectively. Silencing of Rh*PMP1* and Rh*APC3b* in rose plants was conducted as previously described (Wu et al., 2017; Zhang et al., 2019). Briefly, whole plants were submerged in infiltration buffer containing pTRV1 and pTRV2 or its derivatives (OD600 = ~1.0) twice and subjected to vacuum infiltration at −0.8 kg/cm^2, each for 60 s. The plants were washed briefly with distilled water and transplanted into a mixture of 1:1 (v/v) peat:vermiculite. The inoculated plants were grown in a greenhouse at 21 ± 2°C, a relative humidity of ~60%, and 100–120 µmol m^{-2} s^{-1} illumination with fluorescent lamps (SINOL, SN-T5, 16 W) under a 16-h day/8-h night period until observation. Three independent experiments were performed with 60–80 plants per experiment. Phenotypes were checked starting at 35 days after inoculation. The primers are listed in Supplemental Data Set S3.

Gene expression analysis

Total RNA was extracted from rose petals using the hot borate method as previously described (Ma et al., 2006). For reverse transcription-PCR, first-strand cDNA was synthesized from 1 µg of total RNA using Reverse Transcriptase M-MLV (RNase H-) (Takara Biomedical Technology Co., Ltd., Shiga, Japan).

RT-PCR was performed using 1 µL cDNA as template and the Step One Plus real-time PCR system (Applied Biosystems, Foster City, CA, USA) with TaKaRa SYBR Premix Ex Taq II (Takara Biomedical Technology Co., Ltd.). Rh*UBI2* and At*ACTIN2* were used as internal controls for *R. hybrida* and *A. thaliana*, respectively. The cycling parameters were 95°C for 30 s, 40 cycles of 95°C for 5 s, and 60°C for 30 s. The experiments were carried out on three or four independent biological replicates of each sample. All primers used are listed in Supplemental Data Set S3.

Cloning

A partial Rh*PMP1* and Rh*APC3b* sequences were obtained from a rose RNA-seq data set, and the full-length and promoter sequences were obtained using rapid amplification of cDNA ends (Clontech Laboratories, Inc.) and thermal asymmetric interlaced PCR (Takara Biomedical Technology [Beijing] Co., Ltd.) according to the manufacturer's instructions. All PCR products were subcloned into the pGEM-T easy vector (Promega Biotech Co., Ltd., Madison, WI, USA) and transformed into *Escherichia coli* DH5α cells prior to sequencing. All primers used are listed in Supplemental Data Set S3.

Phylogenetic analysis

Amino acid alignment and phylogenetic analysis were performed using ClustalW (https://www.genome.jp/tools-bin/clustalw) and MEGA version 6.0 (Tamura et al., 2013), respectively. The phylogenetic trees were computed using the neighbor-joining algorithm with 10,000 bootstrap replicates. FASTA files for phylogenetic and alignment analysis of Rh*PMP1*, Rh*APC3b*, and Rh*EIN3* are provided in Supplemental Data Set S4.

Subcellular localization in *N. benthamiana*

The Rh*PMP1* ORF containing *Xba* I and *Sal* I restriction sites were inserted into the Super1300 vector at the 5′ end of the sequence encoding green fluorescent protein (GFP) to construct the pSuper:Rh*PMP1-GFP* plasmid. The Rh*APC3b* ORF containing *Xba* I and *Pst* I restriction sites were inserted into the Super1300 vector at the 5′ end of the sequence encoding GFP to generate the pSuper:Rh*APC3b-GFP* plasmid. Subcellular localization of RhPMP1-GFP and RhAPC3b-GFP was analyzed as previously described (Zhang et al., 2019). *Agrobacterium* cells (GV3101) expressing pSuper:Rh*PMP1-GFP* or pSuper:Rh*APC3b-GFP* were re-suspended in

infiltration buffer (10 mM $MgCl_2$, 10 mM MES-KOH, pH 5.6; adding 200 μM acetosyringone immediately prior to use) to an OD_{600} of 0.8. The re-suspended *Agrobacteria* were infiltrated into *N. benthamiana* leaves using 1 ml needleless syringes. The infiltrated leaves were collected 48 h later. Fluorescence signals were detected using a *Nikon* T1 confocal laser-scanning microscope (Nikon, Tokyo, Japan). The excitation wavelengths for GFP and DAPI were 488 and 408 nm, respectively, and the emission filter wavelengths were 505–530 nm for GFP and 420–480 nm for DAPI. All primers used are listed in Supplemental Data Set S3.

Transcriptional activation analysis

A series of truncation fragments of the *RhPMP1* coding sequence containing *Eco*R I and *Sal* I sites were fused to the GAL4-BD in pBD-GAL4 cam vector and subsequently transformed into AH109 yeast as described in the Yeast Protocols Handbook (Clontech Laboratories, Inc.). Yeast cells harboring full-length RhPMP1 or truncated fragments were grown on synthetic dropout medium lacking tryptophan (SD/-Trp) and tryptophan-histidine (SD/-Trp-His). The transcription activity was confirmed using an X-α-Gal staining assay. All primers used are listed in Supplemental Data Set S3.

RNAi in rose callus

For the Rh*EIN3* RNAi construct, two primer sets with different restriction enzyme sites were used to amplify a 391 bp fragment (2,259–2,650 bp in 3′-UTR). One set, with *Asc* I and *Swa* I sites, was digested and inserted in sense orientation into the pFGC1008 vector; the other, with *Pac* I and *Bam* HI sites, was digested and inserted in antisense orientation into the pFGC1008 vector.

The RNAi construct was introduced into *Agrobacterium* strain EHA105 and grown overnight. The bacteria were collected by centrifugation and re-suspended in infiltration solution (MS + 45 g L^{-1} Glucose + 100 μmol L^{-1} Acetosyringone). The bacterial suspension was adjusted with infiltration solution to an OD_{600} = 0.5 and incubated for 2 h at 28°C with shaking (200 rpm). Rose calli were immersed in the bacterial suspension and incubated for 40 min at 28°C with shaking (180 rpm). The calli were briefly washed and dried on sterilized paper towels to remove excess bacterial solution and incubated at 22 ± 1°C in the dark for 3 days without selection. The calli were selected on medium containing 30 mg L^{-1} Hygromycin B for 30 days.

For ACC treatment, the WT and transformed callus were subjected to 50 μM ACC treatment for 24 h.

Arabidopsis transformation

The promoter (−1,860 to −1 bp from the start codon, ATG) of Rh*PMP1* was cloned and inserted into the *Sal* I and *Spe* I sites of pBI121 vector to generate the ProRh*PMP1:GUS* plasmid. The promoter (−1,774 to −1 bp from the start codon, ATG) of Rh*APC3b* was cloned and inserted into the *Sal* I and *Nco* I sites of the pCAMBI1391 vector to generate ProRh*APC3b:GUS*. To construct the pSuper:Rh*PMP1-GFP* overexpression vector, the ORF of Rh*PMP1* was amplified using a pair of primers containing *Xba* I and *Sal* I restriction sites. The PCR products were digested with the corresponding restriction enzymes and inserted into the Super1300 vector at the 5′ end of the sequence encoding GFP. To construct the pSuper:Rh*APC3b-GFP* overexpression vector, the ORF of Rh*APC3b* was amplified using a pair of primers containing *Xba* I and *Pst* I restriction sites. The PCR products were digested with the corresponding restriction enzymes and inserted into the Super1300 vector at the 5′-end of the sequence encoding GFP. ProRh*PMP1:GUS*, ProRh*APC3b:GUS*, pSuper:Rh*PMP1-GFP*, and pSuper:Rh*APC3b-GFP* were introduced into *Agrobacterium tumefaciens* strain GV3101 cells, which were then used to transform *A. thaliana* using the floral dip method (Zhang et al., 2006). Independent transformants were screened on MS basal medium containing 35 mg L^{-1} hygromycin (for pCAMBI1391 and Super1300) or 50 mg L^{-1} Kanamycin (for pBI121). T2 (ProRh*PMP1:GUS* and ProRh*APC3b:GUS*) or T3 (pSuper:Rh*PMP1-GFP* and pSuper:Rh*APC3b-GFP*) plants were used in this study. All primers used are listed in Supplemental Data Set S3.

Statistical analysis

Statistical analysis was performed using Statistical Product and Service Solutions software (IBM Co., Armonk, NY, USA) and GraphPad Prism version 8.0 (GraphPad Software Inc., La jolla, CA, USA: http://www.graphpad.com/). All experimental data were tested with a Student's *t* test, a Mann–Whitney test, or a Duncan's multiple range test. A summary of statistical tests is presented in Supplemental Data Set S5.

Accession numbers

Sequence data from this article can be found in the Arabidopsis Genome TAIR database or GenBank databases under the following accession numbers: Rh*PMP1* (KP058663), Rh*UBI2* (JK618216), Rh*EIN3* (KC484653), Rh*PIP2;1* (EU572717), Rh*APC3b* (MN626999), At*ACT2* (NM_112764), Sl*HB1* (CAP16664.1), Mt*HB1* (XP_003627511), Gm*HB* (ACU24436), Nb*HB1* (ADH04264), Pt*HB* (XP_002302659), Vv*HB* (XP_002262950), Zm*HB* (NP_001183573), At*HB1* (AT3G01470), At*HB3* (AT5G15150), At*HB5* (AT5G65310), At*HB6* (AT2G224300), At*HB7*(AT2G46680), At*HB12* (AT3G61890), At*HB13* (AT1G69780), At*HB16* (AT4G40060), At*HB20* (AT3G01220), At*HB21* (AT2G18550), At*HB22* (AT2G36610), At*HB23* (AT1G26960), At*HB40* (AT4G36740), At*HB51* (AT5G03790), At*HB52* (AT5G53980), At*HB53* (AT5G66700), At*HB54* (AT1G27045), At*HB2* (AT4G16780), At*HB4* (AT2G44910), *HAT1* (AT4G17460), *HAT2* (AT5G47370), *HAT3* (AT3G60390), *HAT9* (AT2G22800), *HAT14* (AT5G06710), At*HB17* (AT2G01430), *HAT22* (AT4G37790), At*HB8* (AT4G32880), At*HB9* (AT1G30490), At*HB14* (AT2G34710), At*HB15* (AT1G52150), *IFL1* (AT5G60690), *GL2* (AT1G79840), At*ML1* (AT4G21750), *ANL2* (AT4G00730), *PDF2* (AT4G04890), *HDG1* (AT3G61150), *HDG2* (AT1G05230), *HDG3* (AT2G32370), *HDG4* (AT4G17710), *HDG5*

(AT5G46880), *HDG6* (AT4G25530), *HDG7* (AT5G52170), *HDG8* (AT3G03260), *HDG9* (AT5G17320), *HDG10* (AT1G34650), *HDG11* (AT1G73360), *HDG12* (AT1G17920), At*APC1* (AT5G05560), At*APC2* (AT2G04660), At*APC3a* (AT3G16320), At*APC3b* (AT2G20000), At*APC4* (AT4G21530), At*APC5* (AT1G06590), At*APC6* (AT1G78770), At*APC7* (AT2G39090), At*APC8* (AT3G48150), At*APC10* (AT2G18290), At*APC11* (AT3G05870), At*APC13* (AT1G73177), At*APC15* (AT5G63135), *Citrus sinensis EIN3-like* (XP_006470438.1), *C. sativus EIN3* (NP_001295791.1), *Populus trichocarpa EIN3* (XP_002312841.3), *Glycine max EIN3* (XP_003543159.1), *Gossypium hirsutum EIN3-like* (XP_016754801.1), *Gossypium barbadense EIN3-like* (KAB2018515.1), *Fragaria vesca EIN3* (XP_004288382.1), and *A. thaliana EIN3* (AAC49749.1). RNA-seq data that support the findings of this study have been deposited in NCBI Bioproject database under accession number PRJNA588150 and in the Rose Transcriptome Database (http://bioinfo.bti.cornell.edu/cgi-bin/rose_454/index.cgi).

Supplemental data

The following materials are available in the online version of this article.

Supplemental Figure S1. Scanning electron microscopy images of petals cut vertically from rose flowers at different stages of opening.

Supplemental Figure S2. Flower opening is associated with the asymmetric growth of petal bases from in vitro cultured rose plants.

Supplemental Figure S3. Ethylene promotes the asymmetric growth of petal bases in rose.

Supplemental Figure S4. 1-MCP prolongs petal movement and flower opening in roses.

Supplemental Figure S5. Ethylene-accelerated outward movement of petals is independent of petal lamina growth.

Supplemental Figure S6. Silencing of Rh*PMP1* impairs ethylene-promoted flower opening and asymmetric growth of ADSP in petal bases.

Supplemental Figure S7. Putative amino acid sequence of RhPMP1 and *cis*-element analysis of the Rh*PMP1* promoter.

Supplemental Figure S8. Identification of Rh*PMP1*-RNAi lines.

Supplemental Figure S9. Knockdown of Rh*PMP1* by RNA interference prolongs natural flower opening in roses.

Supplemental Figure S10. Putative amino acid sequence of RhEIN3 and qRT-PCR analysis of expression of ethylene-responsive gene Rh*ERF003* and Rh*PR10* in response to ethylene in Rh*EIN3*-RNAi callus.

Supplemental Figure S11. Rh*APC3b* is a direct target of RhPMP1.

Supplemental Figure S12. RhEIN3 is a direct upstream regulator of Rh*APC3b* and expression patterns of Rh*APC3b*.

Supplemental Figure S13. Silencing of Rh*APC3b* impairs ethylene-promoted flower opening and asymmetric growth of ADSP in petal bases.

Supplemental Figure S14. Identification of Rh*APC3b*-RNAi lines.

Supplemental Figure S15. Knockdown of Rh*APC3b* by RNA interference prolongs natural flower opening in roses.

Supplemental Figure S16. Overexpression of Rh*APC3b* significantly increases leaf size and the proportion of cells with high ploidy levels in *A. thaliana*.

Supplemental Figure S17. Overexpression of Rh*PMP1* significantly increases leaf size and the proportion of cells with high ploidy levels in *A. thaliana*.

Supplemental Figure S18. Model of ethylene-regulated epinastic movement of rose petals.

Supplemental Movie S1. Time-lapse video showing the opening of rose flowers.

Supplemental Movie S2. Ethylene promotes flower opening in roses.

Supplemental Movie S3. 1-MCP prolongs flower opening in roses.

Supplemental Movie S4. Knockdown of Rh*PMP1* by RNA interference prolongs flower opening during ethylene treatment in roses.

Supplemental Movie S5. Knockdown of Rh*APC3b* by RNA interference prolongs flower opening during ethylene treatment in roses.

Supplemental Data Set S1. List of the ethylene-responsive TFs in petal bases.

Supplemental Data Set S2. List of DEGs in Rh*PMP1*-silenced rose plants.

Supplemental Data Set S3. List of primers used in this study.

Supplemental Data Set S4. FASTA files for phylogenetic and alignment analysis of Rh*PMP1*, Rh*APC3b*, and Rh*EIN3*.

Supplemental Data Set S5. Summary of statistical tests.

Acknowledgments

We thank Dr. De Ye (China Agricultural University) for his generous help in preparing semi-thin sections. We also thank Dr. Ying Bao (Tangshan Normal University) for her generous help in generating transgenic plants and Dr. Zhizhong Gong (China Agricultural University) for providing the pSuper1300 vector and Dr. Dapeng Zhang (Tsinghua University) for his excellent advice. Finally, we thank PlantScribe (www.plantscribe.com) for careful editing of this article.

Funding

This work was supported by the National Key Research and Development Program of China (Grant no. 2018YFD1000400), National Natural Science Foundation of China (Grant no. 31522049 and 31872148), the 111 Project of the Ministry of Education (B17043), and the Construction of Beijing Science and Technology Innovation and Service Capacity in Top Subjects (CEFF-PXM2019_014207_000032).

Conflict of interest statement. None declared.

References

Ariel FD, Manavella PA, Dezar CAChan RL (2007) The true story of the HD-Zip family. Trends Plant Sci **12:** 419–426

Azad AK, Sawa Y, Ishikawa T, Shibata H (2004) Phosphorylation of plasma membrane aquaporin regulates temperature-dependent opening of tulip petals. Plant Cell Physiol **45:** 608–617

Anders S, Huber W (2010) Differential expression analysis for sequence count data. Genome Biol **11:** R106

Blilou I, Frugier F, Folmer S, Serralbo O, Willemsen V, Wolkenfelt H, Eloy NB, Ferreira PCG, Weisbeek P, Scheres B (2002) The *Arabidopsis HOBBIT* gene encodes a CDC27 homolog that links the plant cell cycle to progression of cell differentiation. Genes Dev **16:** 2566–2575

Chao Q, Rothenberg M, Solano R, Roman G, Terzaghi W, Ecker JR (1997) Activation of the ethylene gas response pathway in Arabidopsis by the nuclear protein ETHYLENE-INSENSITIVE3 and related proteins. Cell **89:** 1133–1144

Chen J, Moreau C, Liu Y, Kawaguchi M, Hofer J, Ellis N, Chen R (2012) Conserved genetic determinant of motor organ identity in *Medicago truncatula* and related legumes. Proc Natl Acad Sci USA **109:** 11723–11728

Cheng C, Xu X, Singer SD, Li J, Zhang H, Gao M, Wang L, Song J, Wang X (2013) Effect of GA_3 treatment on seed development and seed-related gene expression in grape. PLoS One **8:** e80044

Cortizo M, Laufs P (2012) Genetic basis of the "sleeping leaves" revealed. Proc Natl Acad Sci USA **109:** 11474–11475

Cote GG (1995) Signal transduction in leaf movement. Plant Physiol **109:** 729–734

Dan H, Imaseki H, Wasteneys GO, Kazama H (2003) Ethylene stimulates endoreduplication but inhibits cytokinesis in cucumber hypocotyl epidermis. Plant Physiol **133:** 1726–1731

Darwin C, Darwin F (1880) The Power of Movement in Plants. John Murray, London

Doležel J, Greilhuber J, Suda J (2007) Estimation of nuclear DNA content in plants using flow cytometry. Nat Protoc **2:** 2233–2244

Eloy NB, de Freitas Lima M, Ferreira PC, Inzé D (2015) The role of the anaphase-promoting complex/cyclosome in plant growth. Crit Rev Plant Sci **34:** 487–505

Forterre Y (2013) Slow, fast and furious: understanding the physics of plant movements. J Exp Bot **64:** 4745–4760

Gendreau E, Orbovic V, Höfte H, Traas J (1999) Gibberellin and ethylene control endoreduplication levels in the *Arabidopsis thaliana* hypocotyl. Planta **209:** 513–516

Harmer SL, Brooks CJ (2018) Growth-mediated plant movements: hidden in plain sight. Curr Opin. Plant Biol **41:** 89–94

Heyman J, De Veylder L (2012) The anaphase-promoting complex/cyclosome in control of plant development. Mol Plant **5:** 1182–1194

Jackson MB (1985) Ethylene and responses of plants to soil waterlogging and submergence. Ann Rev Plant Physiol **36:** 145–174

Kaihara S, Takimoto A (1981) Physical basis of flower-opening in *Pharbitis nil*. Plant Cell Physiol **22:** 307–310

Kang BG (1979) Epinasty. In W Haupt, ME Feinleib, eds, Physiology of Movements. Springerr-Verlag, Berlin, Germany, pp 647–667

Kiss JZ (2000) Mechanisms of the early phases of plant gravitropism. Crit Rev Plant Sci **19:** 551–573

Lang A (1952) Physiology of Flowering. Ann Rev Plant Physiol **3:** 265–306

Liang H, Mahadevan L (2011) Growth, geometry, and mechanics of a blooming lily. Proc Natl Acad Sci USA **108:** 5516–5521

Lin R, Ding L, Casola C, Ripoll DR, Feschotte C, Wang H (2007) Transposase-derived transcription factors regulate light signaling in *Arabidopsis*. Science **318:** 1302–1305

Liscum E, Askinosie SK, Leuchtman DL, Morrow J, Willenburg KT, Coats DR (2014) Phototropism: growing towards an understanding of plant movement. Plant Cell **26:** 38–55

Liu G, Yuan Y, Jiang H, Ning G, Zhao L, Zhou X, Zhou H, Gao J, Ma N (2021) *Agrobacterium tumefaciens*-mediated transformation of modern rose (*Rosa hybrida*) using leaf-derived embryogenic callus. Hortic Plant J doi.org/10.1016/j.hpj.2021.02.001

Lü P, Zhang C, Liu J, Liu X, Jiang G, Jiang X, Khan MA, Wang L, Hong B, Gao J (2014) RhHB1 mediates the antagonism of gibberellins to ABA and ethylene during rose (*Rosa hybrida*) petal senescence. Plant J **78:** 578–590

Ma N, Cai L, Lu W, Tan H, Gao J (2005) Exogenous ethylene influences flower opening of cut roses (*Rosa hybrida*) by regulating the genes encoding ethylene biosynthesis enzymes. Sci China C Life Sci **48:** 434–444

Ma N, Tan H, Liu X, Xue J, Li Y, Gao J (2006) Transcriptional regulation of ethylene receptor and *CTR* genes involved in ethylene-induced flower opening in cut rose (*Rosa hybrida*) cv. Samantha. J Exp Bot **57:** 2763–2773

Ma N, Xue J, Li Y, Liu X, Dai F, Jia W, Luo Y, Gao J (2008) *Rh-PIP2; 1*, a rose aquaporin gene, is involved in ethylene-regulated petal expansion. Plant Physiol **148:** 894–907

Ma N, Chen W, Fan T, Tian Y, Zhang S, Zeng D, Li Y (2015) Low temperature-induced DNA hypermethylation attenuates expression of *RhAG*, an *AGAMOUS* homolog, and increases petal number in rose (*Rosa hybrida*). BMC Plant Biol **5:** 237

Merchante C, Alonso JM, Stepanova AN (2013) Ethylene signaling: simple ligand, complex regulation. Curr Opin Plant Biol **16:** 554–560

Millenaar FF, Cox MCH, van Berkel YE, Welschen RAM, Pierik R, Voesenek LAJC, Peeters AJM (2005) Ethylene-induced differential growth of petioles in Arabidopsis. Analyzing natural variation, response kinetics, and regulation. Plant Physiol **137:** 998–1008

Moran, N. (2015) Rhythmic leaf movements: physiological and molecular aspects. *In* S Mancuso, S Shabala, eds, Rhythms in Plants: Dynamic Responses in a Dynamic Environment. Springer International Publishing, Cham, Switzerland, pp 57–95

Moran N, Yueh YG, Crain RC (1996) Signal transduction and cell volume regulation in plant leaflet movements. Physiology **11:** 108–114

Pérez-Pérez JM, Serralbo O, Vanstraelen M, Gonzalez C, Criqui MC, Genschik P, Kondorosi E, Scheres B (2008) Specialization of CDC27 function in the *Arabidopsis thaliana* anaphase-promoting complex (APC/C). Plant J **53:** 78–89

Palena CM, Tron AE, Bertoncini CW, Gonzalez DH, Chan RL (2001) Positively charged residues at the N-terminal arm of the homeodomain are required for efficient DNA binding by homeodomain-leucine zipper proteins. J Mol Biol **308:** 39–47

Pei H, Ma N, Tian J, Luo J, Chen J, Li J, Zheng Y, Chen X, Fei Z, Gao J (2013) An NAC transcription factor controls ethylene-regulated cell expansion in flower petals. Plant Physiol **163:** 775–791

Pierik R, Tholen D, Poorter H, Visser EJW, Voesenek LACJ (2006) The Janus face of ethylene: growth inhibition and stimulation. Trends Plant Sci **11:** 176–183

Pinon V, Etchells JP, Rossignol P, Collier SA, Arroyo JM, Martienssen RA, Byrne ME (2008) Three *PIGGYBACK* genes that specifically influence leaf patterning encode ribosomal proteins. Development **135:** 1315–1324

Polko JK, Voesenek LACJ, Peeters AJM, Pierik R (2011) Petiole hyponasty: an ethylene-driven, adaptive response to changes in the environment. AoB Plants **2011:** plr031

Polko JK, van Zanten M, van Rooij JA, Marée AF, Voesenek LACJ, Peeters AJM, Pierik R (2012) Ethylene-induced differential petiole growth in *Arabidopsis thaliana* involves local microtubule reorientation and cell expansion. New Phytol **193:** 339–348

Polko JK, van Rooij JA, Vanneste S, Pierik R, Ammerlaan AMH, Vergeer-van Eijk MH, McLoughlin F, Gühl K, Van Isterdael G, Voesenek LACJ et al. (2015) Ethylene-mediated regulation of A2-type CYCLINs modulates hyponastic growth in Arabidopsis. Plant Physiol **169:** 194–208

Reed SI (2003) Ratchets and clocks: the cell cycle, ubiquitylation and protein turnover. Nat Rev Mol Cell Biol **4:** 855–864

Reid MS, Evans RY (1986) Control of cut flower opening. Acta Hortic **181:** 45–54

Reid MS, Evans RY, Dodge LL, Mor Y (1989) Ethylene and silver thiosulfate influence opening of cut rose flowers. J Am Soc Hortic Sci **114:** 436–440

Serralbo O, Pérez-Pérez JM, Heidstra R, Scheres B (2006) Non-cell-autonomous rescue of anaphase-promoting complex function revealed by mosaic analysis of *HOBBIT*, an *Arabidopsis CDC27* homolog. Proc Natl Acad Sci USA **103:** 13250–13255

Song K, Yeom E, Lee SJ (2014) Real-time imaging of pulvinus bending in *Mimosa pudica*. Sci Rep **4:** 6466

Srikanth A, Schmid M (2011) Regulation of flowering time: all roads lead to Rome. Cell Mol Life Sci **68:** 2013–2037

Su SH, Gibbs NM, Jancewicz AL, Masson PH (2017) Molecular mechanisms of root gravitropism. Curr Biol **27:** R964–R972

Tamura K, Stecher G, Peterson D, Filipski A, Kumar S (2013) MEGA6: molecular evolutionary genetics analysis version 6.0. Mol Biol Evol **30:** 2725–2729

van Doorn WG, van Meeteren U (2003) Flower opening and closure: a review. J Exp Bot **54:** 1801–1812

Van Doorn WG, Kamdee C (2014) Flower opening and closure: an update. J Exp Bot **65:** 5749–5757

van Zanten M, Pons TL, Janssen JAM, Voesenek LACJ, Peeters AJM (2010) On the relevance and control of leaf angle. Crit Rev Plant Sci **29:** 300–316

Voesenek LACJ, Bailey-Serres J (2015) Flood adaptive traits and processes: an overview. New Phytol **206:** 57–73

Vreeburg RAM, Benschop JJ, Peeters AJ, Colmer TD, Ammerlaan AHM, Staal M, Elzenga TM, Staals RHJ, Darley CP, McQueen-Mason SJ, Voesenek LACJ (2005) Ethylene regulates fast apoplastic acidification and expansin A transcription during submergence-induced petiole elongation in *Rumex palustris*. Plant J **43:** 597–610

Vriezen WH, De Graaf B, Mariani C, Voesenek LACJ (2000) Submergence induces expansin gene expression in flooding-tolerant *Rumex palustris* and not in flooding-intolerant *R. acetosa*. Planta **210:** 956–963

Wood WML (1953) Thermonasty in tulip and crocus flowers. J Exp Bot **4:** 65–77

Wu L, Ma N, Jia Y, Zhang Y, Feng M, Jiang CZ, Ma C, Gao J (2017) An ethylene-induced regulatory module delays flower senescence by regulating cytokinin content. Plant Physiol **173:** 853–862

Xue J, Li Y, Tan H, Yang F, Ma N, Gao J (2008) Expression of ethylene biosynthetic and receptor genes in rose floral tissues during ethylene-enhanced flower opening. J Exp Bot **59:** 2161–2169

Yamada K, Norikoshi R, Suzuki K, Nishijima T, Imanishi H, Ichimura K (2009) Cell division and expansion growth during rose petal development. J Jpn Soc Hortic Sci **78:** 356–362

Zhang S, Feng M, Chen W, Zhou X, Lu J, Wang Y, Li Y, Jiang CZ, Gan SS, Ma N et al. (2019) In rose, transcription factor PTM balances growth and drought survival via PIP2;1 aquaporin. Nat Plants **5:** 290–299

Zhang X, Henriques R, Lin SS, Niu QW, Chua NH (2006) *Agrobacterium*-mediated transformation of *Arabidopsis thaliana* using the floral dip method. Nat Protoc **1:** 641–646

Zhong S, Joung JG, Zheng Y, Chen YR, Liu B, Shao Y, Xiang JZ, Fei Z, Giovannoni JJ (2011) High-throughput illumina strand-specific RNA sequencing library preparation. Cold Spring Harb Protoc **2011:** 940–949